HHS Public Access

Author manuscript

Glia. Author manuscript; available in PMC 2024 April 01.

Published in final edited form as:

Glia. 2023 April ; 71(4): 926–944. doi:10.1002/glia.24315.

Kir4.1 is specifically expressed and active in non-myelinating Schwann cells

Nicole M. Procacci[1], **Robert Louis Hastings**[3], **Aamir A. Aziz**[2], **Nina M. Christiansen**[2], **Jie Zhao**[1], **Claire DeAngeli**[1], **Normand LeBlanc**[2], **Lucia Notterpek**[1], **Gregorio Valdez**[3], **Thomas W. Gould**[1,*]

[1]Department of Physiology and Cell Biology, University of Nevada School of Medicine, Reno, NV 89557

[2]Department of Pharmacology, University of Nevada School of Medicine, Reno, NV 89557

[3]Department of Molecular Biology, Cell Biology and Biochemistry, Brown University, Providence, RI 02912

Abstract

Non-myelinating Schwann cells (NMSC) play important roles in peripheral nervous system formation and function. However, the molecular identity of these cells remains poorly defined. We provide evidence that Kir4.1, an inward-rectifying K+ channel encoded by the *KCNJ10* gene, is specifically expressed and active in NMSC. Immunostaining revealed that Kir4.1 is present in terminal/perisynaptic SCs (TPSC), synaptic glia at neuromuscular junctions (NMJ), but not in myelinating SCs (MSC) of adult mice. To further examine the expression pattern of Kir4.1, we generated BAC transgenic *Kir4.1-CreER*^{T2} mice and crossed them to the tdTomato reporter line. Activation of CreER^{T2} with tamoxifen after the completion of myelination onset led to robust expression of tdTomato in NMSC, including Remak Schwann cells (RSC) along peripheral nerves and TPSC, but not in MSC. In contrast, activating CreER^{T2} before and during the onset of myelination led to tdTomato expression in NMSC and MSC. These observations suggest that immature SC express Kir4.1, and its expression is then downregulated selectively in myelin-forming SC. In support, we found that while activating CreER^{T2} induces tdTomato expression in immature SC, it fails to induce tdTomato in MSC associated with sensory axons in culture. NMSC derived from neonatal sciatic nerve were shown to express Kir4.1 and exhibit barium-sensitive inwardly rectifying macroscopic K^+ currents. Thus, this study identified Kir4.1 as a potential modulator of immature SC and NMSC function. Additionally, it established a novel transgenic mouse line to introduce or delete genes in NMSC.

Graphical Abstract

*Corresponding Author.

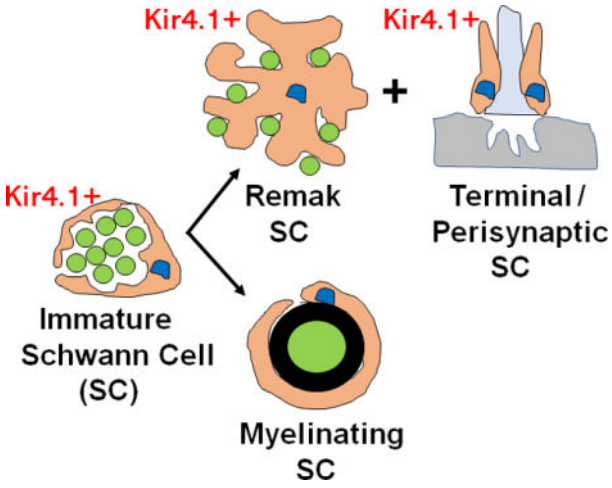

Keywords

Kir4.1; glia; myelination; neuromuscular junction; Schwann cells; synapse

Introduction

Schwann cells (SC) are a subpopulation of neural crest-derived peripheral glial cell that regulate the development, survival, metabolism and function of the axons and synaptic terminals of peripheral neurons (Quintes et al., 2010). In peripheral somatic nerves, SC include myelinating and non-myelinating subtypes. Myelinating SC (MSC) are associated with single axons larger than 1μm in diameter, around which they elaborate the lipid-rich myelin sheath that facilitates the fast rates of electrical signal propagation observed in these axons (Nave and Werner, 2014). In contrast, non-myelinating SC (NMSC) include Remak SC (RSC) that extend cytoplasmic processes around bundles of axons less than 0.5–1.5 μm in diameter, as well as terminal/perisynaptic SC (TPSC) that reside at the neuromuscular junction (NMJ). RSC provide trophic support to small diameter axons including C fiber nociceptors (Harty and Monk, 2017) and play important roles in innervation after peripheral nerve injury (Griffin and Thompson, 2008) and tumorigenesis (Carroll and Ratner, 2008). TPSC regulate synaptic structure (Reddy et al., 2003; Barik et al., 2016; Hastings et al., 2020) and function (Jahromi et al., 1992; Robitaille, 1998; Darabid et al., 2014; Heredia et al., 2018) during development and after injury (Son and Thompson, 1995). MSC and NMSC are also associated with the axons of autonomic nerves. Several additional subtypes of neural crest-derived, non-myelinating peripheral glia appear to be closely related transcriptionally to NMSC, including satellite glial cells (SGC) surrounding the cell bodies of neurons in cranial and spinal sensory ganglia (George et al., 2018) or neuroendocrine cells in the adrenal medulla (Kastriti et al., 2020), as well as enteric glial cells (EGC) surrounding the cell bodies and axons of enteric neurons (Rao et al., 2015).

SC are derived from neural crest precursor cells (NCPC), which express a defined set of genes including *Sox10*, *erbB3* and *L1*, and differentiate into SC precursors (SCP) that invade nascent peripheral nerves of the mouse hindlimb at E12 (Dong et al., 1999). SCP

express a new set of genes in addition to *Sox10*, *erbB3* and *L1*, such as *MBP*, *MPZ* and peripheral myelin protein 22 (*PMP22*; Woodhoo and Sommer, 2008), but depend on axonal signals for survival. In embryonic day 15.5 (E15.5) mice, SCP differentiate into immature SC (iSch) which produce autocrine factors for survival and express a new set of genes, including *GFAP*, *O4* and *S100β*. These cells either form a 1:1 relationship with larger-diameter axons in a process termed radial sorting (Feltri et al., 2016), in which case they become pro-myelinating SC that form compact myelin, or stay in relation with populations of smaller axons, in which case they become RSC (Jessen and Mirsky, 2019). The number of myelinated axons increases most rapidly between P0 and P8, stays constant, then undergoes a second peak in the third postnatal week, with the last changes observed by P30 (Hahn et al., 1987). Although the onset of myelination, as measured by the appearance of new myelinated axons, finishes by P30, myelination itself continues until P60. While the positive and negative molecular pathways underlying the differentiation of MSC are well characterized (Jessen and Mirsky, 2008; 2010), considerably less is known about the differentiation of RSC from iSch, or whether RSCs are essentially iSch that retain the capacity to undergo myelination depending on environmental context.

In order to study the development of RSC from iSch, as well as to evaluate the effect of selectively removing or expressing various genes in RSC on small axon survival, structure and function, it would be useful to generate a mouse Cre-driver tool that is directed exclusively to these cells. However, most of these tools drive expression either in SCP, and therefore iSch and both RSC and MSC (*P0-Cre*; Feltri et al., 1999; *PLP-CreER*^{T2}; Leone et al., 20023; Gomez-Sanchez et al., 2017), mostly but not exclusively in RSC (*Nav1.8-Cre*; Fricker et al., 2009), or in small numbers of RSC (*Egr1-CreER*^{T2}; Sapkota and Dougherty, 2020). Moreover, because RSC may be genotypically the same as iSch, congenital Cre-drivers may fail to achieve RSC-specific expression, as such a tool will also drive expression in MSC based on its earlier activity in iSch. Instead, temporally-inducible Cre may be able to selectively target RSC.

In recent studies of TPSC at the NMJ, we found that motor nerve stimulation regulates extracellular potassium / $[K^+]_o$ homeostasis (Heredia et al., 2018), suggesting that these cells may express several proteins mediating inward fluxes of K^+. This led us to determine whether these cells, similar to other perisynaptic glia, express proteins underlying K^+ import, such as the α2 subunit of the Na^+, K^+ ATPase, encoded by *ATP1a2*, the $Na^+/K^+/Cl^-$ cotransporter (NKCC1), encoded by *SLC12a2*, or the inwardly rectifying K^+ channel Kir4.1, encoded by *KCNJ10*. Constitutive or CNS glial-specific inactivation of the genes encoding each of these proteins disrupts glial cell volume (*SLC12A2*; Su et al., 2002), produces episodic motor paralysis (*ATP1a2*; Smith et al., 2020) and induces ataxia and epileptiform neuronal activity, seizure susceptibility, axon degeneration and reduced muscle force (*KCNJ10*; Djukic et al., 2007; Larson et al., 2018; Schirmer et al., 2018; Kelley et al., 2018). RT-PCR studies showed expression of *KCNJ10*, but not *SLC12a2* or *ATP1a2*, in SC sorted by FACS from muscle. Using a specific antibody for Kir4.1, we detected immunoreactivity in TPSC in a variety of skeletal muscles, but not in skeletal muscle or motor axon terminals. Kir4.1 was also enriched in TPSC in a study by Castro et al. (2020), which utilized several transgenic mouse lines to compare the transcriptional signature of TPSC to that of other SC. Therefore, we sought to further investigate the expression of

Kir4.1 in NMSC, including TPSC, by using a novel transgenic mouse line expressing tamoxifen-inducible Cre recombinase (CreER^{T2}) under the control of the Kir4.1 promoter. We crossed this line to mice expressing the Cre-dependent fluorescent reporter tdTomato to produce *Kir4.1-tdTomato* mice in order to track the spatiotemporal activity of the Kir4.1 promoter following administration of tamoxifen (TMX). In addition, we examined the function of Kir4.1 in NMSC.

In addition to exhibiting expression of tdTomato in TPSC at the NMJ, *Kir4.1-tdTomato* mice treated with TMX at P30, just after the completion of the onset of myelination (~P30), display tdTomato-positive RSC, but not MSC, of peripheral nerve. *In vitro* assays support the idea that myelination downregulates Kir4.1 in SC. Dissociated NMSC from neonatal nerve expressed inwardly rectifying K^+ current, suggesting the presence of functional Kir in these cells. tdTomato expression was also observed in other subtypes of non-myelinating glia throughout the brain and body. Together, these data provide insight into expression of Kir4.1 in glial cells, as well as provide a tool to selectively manipulate NMSC of peripheral nerves.

Materials and Methods

Ethical Approval and Use of Mice:

Sox10-Cre (025807) and conditional Cre-dependent tdTomato (007909) mice were purchased from Jackson Labs (Bar Harbor, ME, US) and maintained in the C57/Bl6 strain. *Kir4.1-CreER^{T2}* mice were generated by Cyagen (Santa Clara, CA, US). Briefly, a CreER^{T2}-polyA cassette, containing Cre fused to the second-generation destabilization domain of the estrogen receptor (ER^{T2}), was inserted via homologous recombination just upstream of the ATG start codon of the *KCNJ10* gene in the BAC RP24–295K5, which contains the mouse *KCNJ10* gene and upstream regulatory sequences. Then two ITR elements, which serve as recognition sites for piggyBAC transposase or PBase, were cloned onto either side of this *KCNJ10-CreER^{T2}* construct by homologous recombination. This construct was then co-injected with PBAse into single cell-stage fertilized embryos from C57BL/6NTac mice for transposition into random TTAA sites of the host genome, with one copy per integration site. Genotyping primers (Forward: 5’-GCCACTGCGGGCTCTACTTCATCG-3’; Reverse 5’-AGCCAGAAGTCAGATGCTTCAAGG-3’) were used to detect the presence of the modified BAC in founder mice. Founder *Kir4.1-CreER^{T2}* mice were crossed to conditional Cre-dependent tdTomato mice (referred to as *Kir4.1-tdTomato* mice) and treated with TMX-containing food for two weeks at different ages postnatally, to induce Cre activity. For embryonic Cre induction, pregnant dams were injected intraperitoneally with TMX dissolved first in ethanol and then in safflower oil for one or two days at 2mg/dose in 100 μl. Animal husbandry and experiments were performed in accordance with the National Institutes of Health *Guide for the Care and Use of Laboratory Animals* and the protocol approved by IACUC at the University of Nevada, Reno.

Drugs:

TMX, barium chloride and L-ascorbic acid (ascorbate) were all purchased from Sigma-Aldrich (St. Louis, MO, US). TMX-containing food (250mg/kg diet) was purchased from Envigo (Indianapolis, IN, US).

Cell Isolation and fluorescence-activated cell sorting (FACS)—The central region of the diaphragm of a P7 *Sox10-tdTomato* mouse was dissected and then placed in Ca^{2+}-free Hank's balanced salt solution (HBSS) containing (in mM): 125 NaCl, 5 KCl, 16 $NaHCO_3$, 0.336 Na_2HPO_4, 0.44 KH_2PO_4, 10 glucose, 2.9 sucrose, and 10 Hepes adjusted to pH 7.4 with NaOH, for 15 min. This endplate band was minced into 1mm-square fragments and placed in a tube of HBSS containing 1% collagenase type 2 (Worthington, Lakewood, NJ, US), 4% bovine serum albumin (Sigma) and 4% trypsin inhibitor (Sigma). The tissue was incubated at 37°C for 30 minutes and then dissociated with fire-polished glass pipette. tdTomato-positive cells from the endplate band were sorted by FACS using a yellow-green excitation laser (561 nm) and bandpass emission filter (585/15 nm). Sorting was performed using a 130 μm nozzle at a sheath pressure of 12 p.s.i. and sort rate of 100 to 2000 events s^{-1}. Live cells, gated on exclusion of the Hoechst 33258 viability indicator, were subsequently gated on tdTomato fluorescence intensity and collected into Trizol reagent (ThermoFisher, Waltham, MA, US).

RT-PCR:

Total RNA from a.) the central "endplate band" region of the diaphragm of postnatal day 7 (P7) wild-type mice, b.) the phrenic nerve of P7 wild-type mice and c.) FACS-sorted cells from the diaphragm endplate band of P7 *Sox10-tdTomato* mice was extracted with Trizol. RNA (1 μg) was treated with DNase and then Superscript 3 reverse transcriptase (ThermoFisher). Semi-quantitative PCR was performed on each of these samples with the following primers: *KCNJ10*: forward: 5'- CTA GTG GCC CCA GGA ATA C-3' and reverse: 5'- CTC TTC TTA GGC CGG GCA AT-3'; *ATP1a2*: forward 5'-GGTGAACTCAGGAGAACGGG-3' and reverse 5'- TGCTTCTTAGCCTACGGTATCC-3'; *SLC12a2*: forward 5'-ACGCAGATGACTTGCGAGAA-3' and reverse: 5'- GGCTGAGTTGGAGTCTTGC-3'. Quantitative PCR was performed on a 96-well CFX Connect (Bio-Rad, Hercules, CA, US) using Sybr Green SSO Advanced 2X Master Mix (BioRad) together with the following primers: *KCNJ10*: forward: 5'- GGA GGA GAT CCT CTG GGG TT-3' and reverse: 5'-CAA CTT GAG CTT CTC GGG GT-3'; *β-actin*: forward: 5'- GGC ACC ACA CCT TCT ACA ATG-3' and reverse: GGG GTG TTG AAG GTC TCA AAC-3'. 40 cycles were run, with each cycle consisting of 10s at 95° C and 30s at 60° C. Fold-changes between cDNA samples prepared as described above from P30 sciatic nerve and spinal cord were quantified using the $2^{-\Delta\Delta C_T}$ method.

Immunohistochemistry:

Mice were anesthetized by intraperitoneal injection of ketamine (100mg/kg) and xylazine (10mg/kg), then perfused transcardially, first with phosphate buffered saline (PBS) and then with 4% paraformaldehyde (Sigma) in PBS. Tissues were dissected, rinsed and

either a.) immersed in 30% sucrose (Sigma) dissolved in PBS, embedded in a 3:2 mix of 30% sucrose/PBS and OCT (Tissue-Tek, Sakura FineTek USA, Torrance, CA, US), flash-frozen in 2-methylbutane (Sigma) on dry ice, and sectioned on a cryostat (CM1850, Leica, Wetzlar, Germany) at 20 μm (spinal cord), 16 μm (nerve, adrenal gland, dorsal root ganglia (DRG), adult diaphragm and extensor digitorum longus (EDL) muscles) or left as whole-mount tissues in PBS (muscle layers of colon after removal of mucosa and submucosa, neonatal diaphragm). Tissue was then incubated overnight at 4°C with antibody solution in PBS containing 0.3% triton-X (0.3% PBST; sections) or 1% triton-X (1% PBST; whole-mounts) and 10% fetal bovine serum (FBS, ThermoFisher). Antibodies against Kir4.1 (rabbit, APC-035, Alomone, Jerusalem, Israel), L1 cell adhesion molecule (L1; rat, clone 324, EMD-Millipore, Burlington, MA, US), APC (mouse IgG_2, CC-1/OP80, EMD-Millipore), NG2 (rabbit, AB5320, EMD-Millipore), IbaI (rabbit, 019–19741, Wako Chemicals, Richmond, VA, US), tyrosine hydroxylase (TH, rabbit, PA5–85167, ThermoFisher), Myelin protein zero (MPZ; chick, PZO, Aves Labs, Davis, CA, US), Myelin basic protein (MBP, chick, CPCA-MBP, EnCor Biotechnology Inc, Gainesville, FL, US), Neurofilament-M (NF-M, chick, 212–901-D84, Rockland Immunochemicals, Pottstown, PA, US), Neurofilament-M (NF-M, mouse, MCA-3H11, EnCor), NeuN (rabbit, ab177487, Abcam, Boston, MA, US), Sox9 (goat, AF3075, R&D systems, Minneapolis, MN, US), S100β (Rabbit, GA50461–2, Agilent, Santa Clara, CA, US), CD31 (rat, 550274, BD Pharmingen, San Jose, CA, US), calbindin-D28K (rabbit, CB38, Swant, Bellinzona, Switzerland) were all used at a dilution of 1/1000 except APC and S100β, which were used at 1/200 and 1/20, respectively. Secondary antibodies (ThermoFisher or Jackson Immunoresearch, West Grove, PA, US) were added to rinsed tissue sections or whole-mounts at 1/400 in 10% FBS/0.3% PBST overnight at 4°C. AlexaFluor 633-, 594- or 488-conjugated α-bungarotoxin (α-BTX; ThermoFisher) was added at a concentration of 1 μg/ml with secondary antibodies. Tissues were confocally imaged with Fluoview software controlling an Olympus FV-1000 laser-scanning fluorescence microscope (Olympus, Tokyo, Japan).

Cell culture and in vitro myelination:

Explant cultures of dorsal root ganglia (DRG) from embryonic *Kir4.1-tdTomato* mice were prepared according to established protocol (Rangarau et al., 2008). Briefly, DRG were excised from embryonic day 15.5 (E15.5) pups and plated on rat tail collagen-coated glass coverslips and maintained in MEM media (ThermoFisher) containing 10% FBS, 0.3% glucose and 50 ng/mL nerve growth factor (NGF; Harlan Bioproducts for Science, Madison, W, USI). In some wells, tamoxifen at a dose determined to be non-toxic (4 μg/ml, dissolved in DMSO) was added to the cultures several days after plating, and then myelination was induced by the addition of 50 μg/ml ascorbate. In other dishes, ascorbate was added first to induce myelination, and then TMX was added one week later. In both cases, coverslips were fixed after 10–14 days of ascorbate treatment, and tdTomato-positive cells imaged by epifluorescence together with mouse NF-M and chick MBP immunofluorescence. For SC cultures, the sciatic nerves of newborn *Kir4.1-tdTomato* mice were dissected, treated with HBSS containing 0.3% Collagenase 2 and 1% DNAse (Worthington) for 30 minutes at 37°C, washed and treated with 0.25% trypsin (MP Biological) for 3 minutes 37°C, rinsed and then dissociated and plated in 1:1 DMEM:F12 media. After one day, cultures were fixed

and tdTomato-positive cells were imaged by epifluorescence together with rabbit S100β immunofluorescence.

Patch Clamp Electrophysiology—The standard whole-cell configuration of the patch clamp technique was used to record macroscopic membrane currents from mouse NMSC (P0 or P1) under voltage clamp conditions. Recordings were obtained with an Axopatch 200B amplifier (Axon Instruments, Sunnyvale, CA), Digidata 1322A data acquisition system (Axon Instruments) and PClamp 9 software (Axon Instruments). The series resistance was compensated to 90% in all experiments. Patch micropipettes with a tip size of 0.8–1.0 μm were fabricated from borosilicate glass (#BF150–110-7.5, Sutter Instruments, Novato, CA) using a P-87 pipette puller (Sutter Instruments, Novato, CA) and fire polished with a MF-830 microforge (Narishige, Tokyo, Japan). An Ag/AgCl pellet connected to ground via the patch clamp amplifier was immersed in the external bath solution (see composition below) and served as the reference electrode. Membrane current or voltage was recorded at a sampling frequency of 1 (ramp protocol or membrane potential) or 5 (step protocol) kHz. All experiments were performed at room temperature.

Freshly isolated SC were seeded on ACLAR 33C Embedding Film (Electron Microscopy Sciences, Hatfield, PA), precut to 6 mm circular autoclaved shards using a standard hole puncher. Approximately 5 to 7 shards containing attached cells were transferred to a 35 mm Petri dish and cultured for 4–6 hours until use in a humified cell culture incubator supplied with 5% CO_2. A single shard containing cells was deposited in a chamber mounted on the stage of an inverted Nikon Eclipse fluorescence microscope (model TE2000-U, Tokyo, Japan) and perfusion with a physiological salt solution (PSS) was initiated at a flow rate of ~ 1 mL/min for ~ 10 min prior to starting the patch clamp experiment. The composition of the PSS (5.4 mM K^+), which served as the Control solution, was as follows (mM): NaCl, 140; KCl, 4.2; KH_2PO_4, 1.2; $MgCl_2$, 1.0; $CaCl_2$, 1.8; Hepes, 5.0; and glucose, 5.5 (pH adjusted to 7.4 with NaOH). For experiments in which the external K^+ solution was increased to 10 mM, 4.6 mM KCl was directly added to the PSS. For the 60 mM K^+-containing solution, 54.6 mM NaCl of the PSS was replaced with an equimolar concentration of KCl. The patch pipette solution used in all experiments had the following composition (mM): K-gluconate, 110; KCl, 30; NaCl, 10; $MgCl_2$, 0.5; Hepes, 5.0; ATP.Mg, 3.0; and EGTA, 5.0 (pH adjusted to 7.2 with KOH).

Immediately after rupturing the membrane to achieve whole-cell recording mode, a short step protocol was imposed to the cell to enable recording of the membrane capacitance (C_m). The protocol consisted in applying 5 consecutive twenty millisecond hyperpolarizing steps from −50 (holding potential, HP) to −60 mV (interval = 22 ms). Capacitative current (I_C) transients generated from these 5 steps were averaged and the mean I_C was integrated to calculate total membrane charge (Q) translocated during the hyperpolarizing step. C_m was then calculated based on the following equation: $C_m = Q/\Delta V$, where |V| was 10 mV. Cell dialysis was then allowed to proceed for 2 min before voltage and current clamp protocols were imposed on the cell. After 2 min of cell dialysis under voltage clamp conditions, the amplifier was switched to current clamp mode to record RMP for 10 s. The cell was then exposed to a short step voltage clamp protocol to generate an I-V relationship that consisted of two hundred millisecond steps ranging from −140 to +60 mV applied in 10

mV increments from HP = −40 mV at a frequency of one step every second. A repetitive voltage ramp protocol was then initiated to monitor changes in membrane current caused by switching to a higher K^+ concentration (10 mM). From HP = −40 mV, the 2-s voltage ramp spanning from −120 to +60 V was applied at a frequency of one ramp every 10 s. Once a stable ramp current was registered in the new condition, the sequence of protocols described above (RMP measurement in current clamp, short step I-V protocol) was repeated. If the gigaohm seal was still intact, the ramp protocol was reinitiated to again monitor changes in membrane current while switching the perfusate to a new solution (e.g., 60 mM K^+ or 60 mM K^+ + 200 μM Ba^{2+} to inhibit Kir4.1). It was not always possible to examine the effects of all K^+ concentrations (and of Ba^{2+} if the seal was still intact) in the same cell due to seal breakdown and therefore some experiments were limited to testing only two K^+ concentrations (5.4 and 10, or 5.4 and 60 mM) to maximize data collection. Resting membrane potential and currents were analyzed using the Clampfit module of PClamp (version 9) and the data were exported to Excel and plotted in OriginPro (version 2021b, Northampton, MA).

Statistics—Results are shown as the mean ± SEM. *n* represents the number of mice and *c* the number of cells or NMJs. The number of male and female samples are also included, and the values from them are pooled, as they did not differ. Unpaired two-tailed Student *t*-tests were used to compare the number of tdTomato+ SC associated with MBP+ axons (TMX after vs. before ascorbate) or the intensity of Kir4.1 immunoreactivity in L1+ or L1− cells of the sciatic nerve. Differences in value were recognized as significant at $p > 0.05$.

Data Availability—All data available upon request at Procacci et al., 2022

Results

TPSC, a subtype of NMSC, express Kir4.1

Since we initiated these studies to find markers of TPSC at the NMJ. we considered that proteins mediating K^+ uptake might represent suitable targets, based on earlier observations that postnatal TPSC exhibit an inwardly directed K^+ flux pathway (Heredia et al., 2018). Candidate proteins for carrying such ion transport include the Na^+, K^+ ATPase (encoded by *ATP1a2*), the $Na^+/K^+/Cl^-$ cotransporter (*SLC12a2*), and the inwardly rectifying K^+ channel Kir4.1 (*KCNJ10*). However, the expression of these proteins in RSC or TPSC has not been reported. RNA from the phrenic nerve of P7 wild-type (WT) mice, from the endplate region of P7 wild-type diaphragm muscle, and from SC sorted by FACS from P7 diaphragm muscle of mice expressing the fluorescent reporter tdTomato in all SC (*Sox10-tdTomato* mice), was subjected to RT-PCR with primers complementary to mouse *SLC12A2*, *ATP1a2*, and *KCNJ10* transcripts. Although SC sorted from the muscle include both SC associated with peripheral nerve branches as well as TPSC at the NMJ, by comparing expression in this sample to that in proximal nerve trunk samples, we could determine whether expression in this sample might be specific to TPSC. *SLC12A2* and *KCNJ10* but not *ATP1a2* were expressed by nerve-derived SC, but only *KCNJ10* expression was detected in SC sorted by FACS from the muscle (Figure 1A). Therefore, we examined expression of the *KCNJ10* gene product Kir4.1 in nerve and muscle by immunohistochemistry. Cross-sections

of diaphragm muscle exhibited robust Kir4.1 immunoreactivity at fluorescently-labeled α-bungarotoxin (α-BTX)-positive acetylcholine receptor (AChR) clusters at the NMJ (Figure 1A). In order to confirm that the expression of Kir4.1 at the NMJ was of perisynaptic glial origin and not derived from presynaptic or postsynaptic elements, NMJ of diaphragm muscle in *Sox10-tdTomato* were stained with Kir4.1 antibody, as both this antibody and the antibody against S100β, a protein expressed by TPSC at the NMJ, are generated in rabbit. Kir4.1 immunoreactivity was detected in tdTomato-positive (tdTom+) TPSC identified by their localization to fluorescent α-BTX-labeled AChR clusters, but not in tdTom+ SC in phrenic nerve branches (Figure 1B). This data is corroborated by RNA-Seq data collected from TPSC isolated by a transgenic approach (Castro et al., 2020); Kir4.1 was expressed 3.3-fold higher in TPSC vs. other SC in skeletal muscle (e.g., RSC and MSC along intramuscular branches; $P<0.0001$) and 7.1-fold higher in TPSC vs non-SC in skeletal muscle ($P<0.0001$). However, Kir4.1 immunoreactivity was also apparent in a punctate pattern in cells expressing the RSC marker L1 cell adhesion molecule (L1; Faissner et al., 1984) in longitudinal sections of the sciatic nerve (Figure 1D).

To determine whether Kir4.1 indeed specifically labels TPSC at the NMJ and not SC in peripheral nerves, kranocytes / parajunctional fibroblasts of the NMJ, motor neurons innervating the NMJ, or skeletal muscle cells, we generated bacterial artificial chromosome (BAC) transgenic mice expressing $CreER^{T2}$ under the control of *KCNJ10* regulatory sequences (Figure 2A). These mice were crossed to mice conditionally expressing tdTomato in the Rosa26 locus to produce double transgenic *Kir4.1-tdTomato* offspring. When these mice were not treated with TMX to stabilize ER and thus activate Cre, no tdTomato-positive (tdTom+) cells were detected in nerve or muscle (Figure 2C). In contrast, when post-weaning stage *Kir4.1-tdTomato* mice (P30) were fed TMX-containing chow for 2 weeks and evaluated one week later, tdTom+ cells were found in diaphragm whole-mount preparations in the central endplate band at fluorescent α-BTX-labeled AChR clusters (Figure 3A). Similar to results above from *Sox10-tdTomato* mice, tdTom+ cells at diaphragm NMJs in *Kir4.1-tdTomato* mice co-labeled with an antibody against S100β, confirming their identity as TPSC (data not shown). tdTom-expressing TPSC at NMJ exhibited Kir4.1 immunoreactivity that was more closely associated with AChR clusters than the tdTom-filled soma of these cells, consistent with its proposed role in regulating synaptic function (Figure 3B). The percentage of AChR clusters in the diaphragm, a muscle containing multiple muscle fiber subtypes, containing tdTom+ cells was 83.4 ± 4.8% (n=5; 2M,3F; c=35/n). We also examined TPSC in the extensor digitorum longus (EDL), a muscle exclusively containing fast-fatigable muscle fibers. Fewer TPSC were tdTom+ in this muscle (49.5 ± 11.5%; n=5; 2M,3F; c=35/n). These data suggest that Kir4.1 is expressed by TPSC at the NMJs of muscles with distinct fiber subtypes, although some variability in the percentage exists between muscles.

RSC, a subtype of NMSC, express Kir4.1

We noticed that in addition to these tdTom+ TPSC, diaphragm whole-mount preparations contained tdTom+ cells in a region of the diaphragm consistent with the location of the phrenic nerve trunk (Figure 3A). However, the number of these cells was considerably less than the number of tdTom+ cells typically observed in that region of the diaphragm

of *Sox10-tdTomato* mice, which drive expression of tdTom in both MSC and RSC of the nerve as well as TPSC of the NMJ (data not shown). Consistent with this observation, expression of *KCNJ10* was detected by qPCR in samples of the sciatic nerve derived from P30 wild-type mice (peak fluorescence observed at 29.3 ± 2.8 cycles, *n*=1M, 2F). However, when compared to samples of spinal cord from these same mice, expression was 6.15 ± 1.3-fold lower in nerve-derived samples. In addition to MSC and RSC, peripheral nerves contain endoneurial, perineurial and epineurial fibroblasts, macrophages and cells associated with blood vessels (Gerber et al., 2021). Hence, we decided to investigate the identity of these cells in cross sections of the sciatic nerve, which contains several thousand myelinated axons and many more unmyelinated axons, and is thus considerably easier to manipulate for immunohistochemical purposes than the phrenic nerve, which only contains ~300 myelinated axons. Consistent with the finding of labeled cells in the trunk region of diaphragm whole-mounts, sciatic nerve cross-sections contained many tdTom+ cells after TMX treatment from P30-P43, just after the completion of the onset of myelination. These tdTom+ cells were completely co-labeled with L1, although not every L1+ cell expressed tdTom (L1+ = 98±2% of tdTom+ cells; tdTom+ = 77±8% of L1+ cells *n*=5; 3M,2F; *c*=125 Figure 4A). In contrast, tdTom+ cells of the sciatic nerve did not co-label with the MSC marker myelin protein zero (MPZ) after this time course of TMX treatment (Figure 5A). Thus, at a time after which the differentiation of iSch into MSC has finished, Kir4.1 expression was not detected within these cells, but rather within L1+ RSCs, as well as S100β+ TPSC at the NMJ. tdTom+ cells were not detected at any appreciable level in other cell types within the nerve, such as NG2+ fibroblasts, Iba1+ macrophages, or CD31+ endothelial cells (Figure 4C), nor in S100β-negative cells at the NMJ (e.g., kranocytes), presynaptic motor axons innervating the NMJ, or other cell types in skeletal muscle, save small cells associated with superficial axons of the muscle, which are likely NMSC along sympathetic efferent axons innervating blood vessels (data not shown, but see section below on SC associated with sympathetic splenic axons).

The expression of Kir4.1 in RSC but not MSC in the peripheral nerves of young adult mice could reflect *de novo* expression in RSC at P30, or continued expression through the transition from iSch to RSC. In the former scenario, TMX delivery to *Kir4.1-tdTomato* mice younger than P30 would fail to produce significant numbers of tdTom+ MSC or RSC. In the latter case, such TMX delivery would produce tdTom+ cells in each of these subtypes, as they are both derived from iSch. Therefore, we added TMX to mice to induce Cre activity at several timepoints: E13.5, when SCP differentiate from NCPC, E15.5, when iSch differentiate from SCP (Jessen and Mirsky, 2005), E17.5-E18.5, just prior to the period of myelination, P0-P10, prior to and during the peak period of myelination, and P9-P22, after the peak but before the end of myelination and examined cross sections of sciatic nerves at P50 for tdTom+ cells (Figure 2B). Similar to TMX treatment starting at P30, TMX treatment from P9-P22 resulted in tdTom+ cells that were mostly labeled with L1 antibodies (L1+ = 89±8% of tdTom+ cells; *n*=5; 2M,3F; *c*=89; Figure 4). However, a few tdTom+ cells were also labeled with MPZ antibodies (MPZ+ = 11±7% of tdTom+ cells; *n*=5; 2M,3F; c=89; Figure 5). These results support the idea that iSch express Kir4.1 during the postnatal period, since both a small subpopulation of MSC as well as most RSC express tdTom at P50 after TMX treatment during this period.

Next, we examined sciatic nerves at P50 after TMX administration from P0-P10, the period immediately before and during which most peripheral axons begin to myelinate (Hahn et al., 1987). The vast majority of tdTom+ labeled cells expressed MPZ, although some expressed L1 (MPZ+ = 92±4% of tdTom+ cells; L1+ = 7±6% of tdTom+ cells; *n*=4; 2M;2F; c=142 Figures 4–5), suggesting that these cells likely expressed Kir4.1 as iSch. To determine whether Kir4.1 was expressed at earlier stages in NCPC, TMX was injected into dams at E13.5, E15.5 or E17.5-E18.5 and sciatic nerves examined at P50. After injection at E13.5, no tdTomato+ cells were observed in the sciatic nerve at P50 (data not shown). After E15.5 injection, a very small number of tdTom+ cells were detected, all of which were MPZ-immunoreactive, indicating that SC first express Kir4.1 at this iSCh stage (Figures 4–5). Finally, when TMX was injected into dams at E17.5 and at E18.5 and SC from sciatic nerves were cultured from P0 pups, the majority of S100β+ cells were tdTom+ (tdTom+ = 77±4% of S100β+ cells; *n*=3; 1M;2F; *c*=99; Figure 2D). Taken together, these studies suggest that Kir4.1 first becomes expressed by iSch, which then lose expression of Kir4.1 as they differentiate into MSC, or maintain expression as they become RSC.

In order to directly test whether myelination downregulates the expression of tdTom from *Kir4.1-CreER*^{T2} mice, we performed *in vitro* myelination assays of SC derived from embryonic *Kir4.1-tdTomato* mice. Explant cultures of DRG were given TMX either before or after the addition of ascorbic acid to induce myelination, and SC were examined for tdTom expression two weeks later. In response to TMX before ascorbate treatment, MBP-immunoreactive SC associated with sensory axons robustly expressed tdTom; in contrast, when TMX was not delivered to these explant cultures until after the cessation of ascorbate treatment, far fewer MBP-immunoreactive SC expressed tdTom (tdTom+ = 91±4% vs. 12±7% of MBP+ SC adjacent to NF-M+ axons, TMX before vs. after ascorbate, P=0.0003; *n*=3; 1M;2F; *c*=13; Figure 6). These results support the idea that the genetic pathway underlying myelination downregulates the *KCNJ10* gene encoding Kir4.1 in SC.

NMSC express functional Kir

In order to confirm that expression of Kir4.1 in iSch and RSC, as determined by genetic lineage tracing and immunohistochemistry, correlates with functional Kir4.1 protein, we recorded whole-cell currents in these cells dissociated from P0 nerves. The standard whole-cell configuration of the patch clamp technique experiments was used to determine the profile of macroscopic K^+ currents generated by these cells at room temperature. The bath and pipette solutions were devised to simulate Na^+ and K^+ gradients normally experienced by these cells *in vivo*. The inclusion of the Ca^{2+} chelator EGTA (5 mM) in the pipette solution minimized the activity of Ca^{2+}-activated ion channels. Under these conditions, the membrane capacitance and resting membrane potential (RMP) respectively averaged 10.9 ± 0.8 pF (*n*=5; 2M;3F; *c*=18) and −66 ± 3 mV (*n*=4; 2M;2F; *c*=6). Both voltage step and ramp protocols were used to measure membrane currents under voltage clamp conditions. Figure 7A shows four families of membrane currents recorded in the same cell in four different conditions using the short step (200 ms) protocol shown below the traces. In all experiments, the holding potential was set to −40 mV. With normal 5.4 mM $[K^+]_o$, the current was mainly time-independent with the exception of those recorded at very negative potentials (< −120 mV), which displayed a small activation phase followed by a slower time-dependent

decaying phase. Relatively weak inward rectification was apparent with larger currents at negative relative to positive potentials, an effect that saturated at hyperpolarized potentials (notice traces overlapping). Increasing $[K^+]_o$ to 10 mM increased both the inward and outward currents with evidence of currents decaying over time at potentials positive to −40 mV, and at potentials negative to −110 mV. These effects were accentuated when the cell was incubated with 60 mM $[K^+]_o$. We next tested the effects of 0.2 mM Ba^{2+}, a potent inward K^+ channel blocker (Schram et al., 2003; Madadi et al., 2021). Barium blocked both the inward and outward currents, but was much more potent at blocking the inward current (93% vs. 16%), indicating voltage-dependent block. We next plotted in Figure 7B–C the current measured at the end of the pulse (indicated by colored circles in panel A) from this experiment as a function of step potential for these four conditions. These I-Vs highlight the prominent inward rectification of the current, strong dependence of the inward and outward current on $[K^+]_o$ characterized by the marked increase in slope conductance in the negative range of membrane potential, the positive shift in reversal potential as expected for K^+ channels (panel B), and the strong voltage-dependent block produced by Ba^{2+} (Figure 7C). All these effects were also noticeable from analysis of I-Vs produced by a slow voltage ramp protocol (Figure 7D). Mean I-Vs for experiments measured under identical conditions to those of the experiment described in Figure 7A–D revealed a similar profile (Figure 7E–F). Taken together, these properties are typical of a major contribution of inward rectifier K^+ channels (Nichols and Lopatin, 1997; Weaver and Denton, 2021) in this cell type and are likely produced by the activity of Kir4.1 channels (Olsen and Sontheimer, 2008; Nwaobi et al., 2016), which are abundantly expressed in these cells as described earlier. Finally, Figure 7G shows that raising $[K^+]_o$ depolarized the cells in manner approaching Nernstian behavior (blue solid line; slope = 49.4 mV/decade) when compared to the theoretical Nernst potential for K^+ in our conditions (E_K; solid red line), which supports the notion that Kir4.1 channels play a major role in determining RMP in these cells.

SGC of peripheral ganglia, NMSC of autonomic nerves and EGC of the ENS express Kir4.1

We next examined the expression of tdTom+ cells in other regions of the PNS, including the autonomic and enteric nervous systems (ANS, ENS). Within spinal sensory ganglia and the adrenal gland of the PNS, NMSC / satellite glial cells (SGC) that express S100β are found adjacent to the soma of sensory neurons and adrenal chromaffin cells, respectively. These cells robustly expressed Kir4.1 protein as well as tdTom in *Kir4.1-tdTomato* mice (Figure 8). We then examined autonomic nerves of the PNS. The preganglionic parasympathetic vagal nerves contain both myelinated and unmyelinated axons and exhibited fluorescence under the dissecting microscope, as were many other peripheral nerves (data not shown). Cross sections of the right vagal trunk at the level of the esophagus just anterior to the diaphragm expressed tdTom+ cells that co-expressed L1 but not MPZ (Figure 9A). Postganglionic sympathetic nerves are noradrenergic and unmyelinated. Under the dissecting microscope, we observed that the nerve innervating the spleen was fluorescent. Cross sections of this nerve showed tdTom+ cells surrounding tyrosine hydroxylase (TH)+ and neurofilament M+ axons (Figure 9B), indicating that these non-myelinating glia also express Kir4.1. Next, we examined the myenteric ganglia of the ENS, which contains enteric neurons that regulate gut motility and non-myelinating enteric glial cells (EGC) next to the soma of these neurons, similar to the relationship between SGC and neurons in peripheral sensory ganglia, as

well as non-myelinating EGC associated with the axons of these neurons. In whole-mount preparations of the colon stripped of the mucosal and submucosal layers, robust tdTom expression was observed throughout the myenteric ganglia. These tdTom+ cells were positive for the EGC marker S100β but not the neuronal marker NeuN (Figure 9C). In addition to these cells within the ganglia, tdTom+, S100β co-labeled cells were detected along the muscle layer innervated by enteric neurons, and were thus likely EGC along axons, as they did not co-express PDGFRα or Kit, which label post-junctional cell types that contribute to the myogenic component of gut motility (data not shown; Sanders et al., 2014). Finally, we investigated tdTom expression in the mucosa of the colon, which contains EGC that form a network and contribute to the intestinal epithelial barrier (Savidge et al., 2007). tdTom+ cells were observed in a network and co-labeled with S100β, confirming that mucosal EGCs also express Kir4.1. Additionally, a population of S100β-negative cells were also tdTom+ in the colonic mucosa (Figure 9D). Interestingly, parietal cells of the gastric mucosa express Kir4.1 (Song et al., 2011), but whether a colonic mucosal epithelial subtype also expresses this channel is unknown. Together, these results show that Kir4.1 is widely expressed in NMSC throughout the PNS, including RSC in somatic nerves, NMSC in autonomic nerves, TPSC, SGC and EGC.

Macroglia of the CNS express Kir4.1

We next investigated the distribution of Kir4.1 in the CNS. Kir4.1 expression has been previously reported in astrocytes (Higashi et al., 2001; Tang et al., 2009), oligodendrocyte precursor cells (OPC; Maldonado et al., 2013; Song et al., 2018; Larson et al., 2018) and oligodendrocytes (OL; Neusch et al., 2001; Kalsi et al., 2004; Brasko et al., 2017). Cross sections of the ventral spinal cord from P50 *Kir4.1-tdTomato* mice fed TMX food from P9-P22 were stained with antibodies against Sox9, NG2 and APC to label astrocytes (Sun et al., 2017), OPC (Nishiyama et al., 1996) and mature OL (Bin et al., 2016), respectively. Low-magnification images of the spinal cord and high-magnification images of the dorsal horn (DH), ventral horn (VH) and ventral white matter (WM) show that nearly all Sox9+ astrocytes in each of these regions express tdTom (tdTom+ = 96 ± 3% of Sox9+ astrocytes, n=5; 2M;3F; c=183; Figure 10A).

NG2+ OPC and CC-1+ OL also each expressed tdTom in *Kir4.1-tdTomato* mice (tdTom+ = 84 ± 14% of NG2+ OPC, n=4; 2M;2F; c=65; tdTom+ = 54 ± 5% of CC-1+ OL; n=4; 2M;2F; c=54; Figure 10B). In contrast to iSch, which stop differentiating into MSC in normal adult nerves by P30, OPC persist and differentiate into OL throughout adulthood, making it difficult to determine whether labeled OL expressed Kir4.1 during TMX treatment or whether they represent OPC which expressed Kir4.1 during treatment that then differentiated into OL after TMX but before sacrifice. In order to address this, we also quantified the percentage of CC-1+ OL that expressed tdTom after administration of TMX at later stages, when OPC turnover into OL is reduced. This number was 47.3 ± 7.1% (n=3; 1M;2F; c=39) when TMX was given from P45-P60, suggesting that OL continue to express this channel after they differentiate from OPC (Figure 10D). We also examined microglia in the spinal cord by immunostaining with Iba1 antibodies. tdTom+ cells did not co-express Iba1, suggesting that microglia are not a source of Kir4.1. RNA collected from Sim-A9 cells, an immortalized mouse microglial cell line, also failed to show evidence of

Kir4.1 expression by RT-PCR (data not shown). Finally, tdTom+ cells did not co-localize with the pan-neuronal marker NeuN (data not shown), confirming previous observations (Tang et al., 2007). Together, these expression studies show that Kir4.1 is expressed by most central and peripheral non-myelinating glial cells, as well as by mature, myelinating OL.

Renal epithelial cell subpopulations express Kir4.1

Finally, we examined the expression outside of the nervous system. Renal expression of Kir4.1 has been extensively reported in the late thick ascending limb (TAL), the distal convoluted tubule (DCT), the connecting tubule (CNT), and the initial connecting duct (CCD; Su and Wang, 2016), and loss-of-function mutations in *KCNJ10* lead to impaired K^+ homeostasis. We stained cross sections of the kidney of *Kir4.1-tdTomato* mice that had been given TMX from P30-P43 with antibodies against the cytosolic calcium-binding protein calbindin-D28K, which is selectively expressed in the DCT (Bindels et al., 1991). We observed extensive, but not complete, co-labeling of tdTom+ cells (calbindin-D28K+ cells = 68 ±12% of tdTom+ cells; tdTom+ cells = 97.7 ± 1.2% of calbindin-D28K+ cells; n=3; 1M;2F; c=38), consistent with the wider expression pattern of Kir4.1 than calbindin-D28K (Figure 11). These results demonstrate that *Kir4.1-CreER^{T2}* mice direct expression to distinct renal epithelial cell subpopulations that have previously been shown to express Kir4.1. Taken together, these studies show that *Kir4.1-CreER^{T2}* mice are a valuable tool to track the cell populations that express Kir4.1 as well as manipulate these cells through genetic techniques. In addition, we confirmed through immunohistochemical and patch clamp recording studies that NMSC express functional Kir4.1 protein, a finding which opens the door for more detailed biophysical as well as genetic studies of the role of Kir4.1 in these cells.

Discussion

Based on previous work demonstrating that TPSC regulate perisynaptic $[K^+]_o$ at the NMJ (Heredia et al., 2018), we sought to determine whether a.) these perisynaptic, non-myelinating glial cells expressed proteins that regulate inward K^+ flux and b.) such expression, if any, was restricted to these cells and not SC along peripheral nerves. TPSC expressed *KCNJ10*, the gene encoding the inwardly rectifying Kir4.1 protein, by RT-PCR and immunohistochemistry. However, *Kir4.1-tdTomato* mice treated with TMX after the completion of myelination exhibited tdTom+ cells not only in TPSC at the NMJ, but also in L1+ RSC of the nerve. Because of the remarkable selectivity of this expression pattern, we focused on characterizing its onset and regulation, as well as whether this pattern produced functional Kir4.1 channels in NMSC.

Several lines of evidence suggest that *KCNJ10*, the gene encoding Kir4.1, initially becomes expressed by iSch and then persists in RSC. First, when a single dose of TMX was given to *Kir4.1-tdTomato* mice at E15.5, when iSch begin to differentiate from SCP, a small number of MPZ+ MSC was observed at P50. Second, when TMX was given slightly later (E17.5-E18.5), at a time when the iSch pool had grown in size, most S100β-expressing NMSC expressed tdTom in P0 sciatic nerve-derived cultures. Third, depending on when TMX was administered postnatally, either just before and during the peak period of myelination

(P0-P10), or after the completion of myelination onset (P30–43), tdTom expression was observed mostly in MSC or exclusively in RSC, respectively. This is consistent with *KCNJ10* expression by a precursor cell capable of differentiating into either of these two mature SC subtypes. Fourth, tdTom+ cells were not observed in the nerve when TMX was administered at E13.5, when SCP have formed from NCPC, but before iSch have formed from SCP. This finding is consistent with the absence in *Kir4.1-tdTomato* mice of tdTom+ fibroblasts of the perineurium of the sciatic nerve (Parmantier et al., 1999), or tdTom+ enteric neurons or vagal neurons (Uesaka et al., 2015, Espinosa-Medina et al., 2017), all of which are derived from SCP. Finally, when TMX was given to cultured SC to myelinate sensory axons in culture, tdTom was not observed in MSC. Together, these observations indicate that *KCNJ10* is initially expressed by iSch and then downregulated in MSC of the nerve, or maintained in RSC of the nerve and TPSC of the NMJ. The relatively high recombination efficiency within RSC and TPSC, together with the absence of expression in MSC or other cell types of the nerve, motor axons or muscle, upon treatment of *Kir4.1-tdTomato* mice with TMX after P30, also suggests that *Kir4.1-CreER*^{T2} mice represent a useful tool to a.) express or delete genes in all SC after early TMX, b.) express or delete genes selectively in RSC and TPSC after late TMX, c.) examine the period of myelination itself by modulating the time course of TMX treatment or d.) examine the fate or RSC after injury or in disease.

In addition to each of these subpopulations of NMSC, tdTom+ cells were observed in every population of non-myelinating glial cell examined except microglia, including NMSC of parasympathetic and sympathetic nerves, SGC of sensory ganglia and adrenal gland, EGC in the smooth muscle and mucosa of the gut, and astrocytes and OPC of the central nervous system (CNS). CNS expression of Kir4.1, which was cloned in 1995 as a CNS glial-derived inwardly rectifying K^+ channel (Takumi et al., 1995), has been extensively examined. Most reports suggest that this protein is expressed by subsets of astrocytes (Poopalasundaram et al., 2000; Higashi et al., 2001) if expressed by any at all (Neusch et al., 2001). Similarly, Olsen et al. (2007) and Kelley et al. (2018) found evidence of selective expression of Kir4.1 in ventral vs. dorsal horn astrocytes or in astrocytes associated with the soma of motor neurons innervating fast vs. slow-twitch muscle fibers, respectively. In contrast, we observed that Kir4.1 was expressed by nearly all Sox9+ astrocytes in both white and gray matter regions. One possible source of this discrepancy is the extensive immunoreactivity of Kir4.1 that is observed throughout the processes of astrocytes, which overlaps with the processes of adjacent astrocytes and complicates its assignment to a precise cellular origin. Moreover, the markers used to label astrocytes in most studies, such as GFAP, preferentially label these processes. In contrast, tdTom expression in the current study was strongest in the soma of labeled cells of *Kir4.1-tdTomato* mice, and these cells could be easily identified as astrocytes with the nuclear marker Sox9, as OL with the cell body marker APC, or as OPC with the cell body and process marker NG2.

In contrast to SC, both OPC and myelinating OL expressed tdTom in *Kir4.1-tdTomato* mice, indicating that myelination differentially regulates Kir4.1 expression in OL vs. SC. Myelination itself requires common and distinct transcriptional regulators in SC vs. OL (Hornig et al., 2013), and the expression of key myelin-associated proteins includes common proteins such as MBP and those specific to OL (proteolipid protein 1; PLP1) or SC

(MPZ, peripheral myelin protein 22; PMP22). One potential mediator of these differential expression patterns is microRNA, species of small noncoding RNA that regulate gene expression. For example, miR-9 is expressed in OL but not SC and represses the expression of PMP22 in these cells (Lau et al., 2008). Although miR 5096 and 205 downregulate Kir4.1 expression in glia (Thuringer et al., 2017; Rivera-Aponte et al., 2020), neither of these has been reported in SC. Alternatively, gene networks driving myelination in SC but not OL may methylate different genes (Arthur-Farraj et al., 2020); methylation of *KCNJ10* inhibits its expression (Nwaobi et al., 2014). Alternatively, tdTom+ OL could reflect Kir4.1 expression in OPC that differentiated into OL subsequent to TMX administration, as the period of OPC differentiation into OL is not restricted to a finite period of time, as is iSch differentiation into MSC. However, the abundant reports of Kir4.1 expression and function in OL support the interpretation that the presence of tdTom+ OL reflects ongoing Kir4.1 expression in these cells (Poopalasundaram et al., 2000; Neusch et al., 2001; Kalsi et al., 2004; Brasko et al., 2017; Larsen et al., 2018; Schirmer et al., 2018).

In order to characterize the biophysical function of Kir4.1in NMSC, we carried out whole cell recording of these cells isolated from P0 sciatic nerve, which would be expected to include a combination of iSch and RSC, as well as nascent MSC which lose their myelin upon dissociation. NMSC displayed biophysical properties consistent with those of Kir4.1 including: a.) negative RMP (average ~ −66 mV) in the presence of normal $[K^+]_o$ (5.4 mM), b.) barium-sensitive inwardly rectifying K^+ currents in response to hyperpolarizing voltage steps and c.) larger inward currents in response to elevated $[K^+]_o$. These findings suggest that K^+ released by active motor axons along the nerve and/or at the NMJ, like exogenous K^+, depolarizes NMSC, similar to classic observations in the salamander optic nerve (Orkland et al., 1966). This glial response to neuronal activity, together with the glial resting membrane potential near the K^+ equilibrium potential (E_K), formed the basis for the glial K^+ spatial buffering hypothesis, in which K^+ is transferred by glia from regions with high to low $[K^+]_o$ (Orkland, 1980). In this model, perisynaptic glia, where $[K^+]_o$ is high as a result of neuronal activity, are connected in an electrical syncytium via gap junctions to perivascular glia, where $[K^+]_o$ is low as a result of efflux into the circulation. K^+ redistribution from the synapse to the vasculature is favored by this syncytium because the elevated K^+ outside the presynaptic glial cell, together with its constant removal from inside this cell, raises E_K above the resting membrane potential (RMP), thus providing the driving force for K^+ influx. Supporting this model of passive K^+ redistribution, the greatest K^+ channel expression and conductances are observed in the perisynaptic and perivascular processes on either end of this syncytium (Newman, 1984; Hibino et al., 2004). However, the extent to which perisynaptic glial K^+ uptake occurs by Kir4.1-mediated spatial buffering, K^+ symport (e.g., $Na^+/K^+/Cl^-$) or K^+ pumping (e.g., Na^+/K^+ ATPase) mechanisms remains controversial (Beckner, 2020). Moreover, the extent to which RSC or TPSC spatially buffer K^+ away from small diameter axons of nerves or the NMJ is unclear, as the expression of gap junctions by these cells, as well as their anatomical relationship to the vasculature, is not well defined. Moreover, the RMP measured from NMSC in this study was always more positive than E_K when $[K^+]_o$ was raised in the range of 5.4 to 60 mM.

Alternatively, the effects of Kir4.1 on glial function may extend beyond its role in K^+ uptake. For example, in mice genetically lacking Kir4.1 or treated with barium, although

glial K^+ uptake is inhibited, glial RMP is also markedly depolarized (Kofuji et al., 2000; Djukic et al., 2007), demonstrating its role in K^+ efflux. This depolarization in turn reduces the driving force for glutamate uptake in astrocytes (Kucheryavykh et al., 2007; Djukic et al., 2007), which elevates perisynaptic glutamate levels and thus result in subsequent excitotoxicity to neurons. Mice lacking Kir4.1 exhibit ataxia, seizure-like activity and sensorineural deafness (Kofuji et al., 2000; Marcus et al., 2002; Djukic et al., 2007; Kucheryavykh et al., 2007). These phenotypic disturbances also occur in humans with loss-of-function mutations in *KCNJ10* and underlie a disease referred to as SeSAME (Seizures, sensorineural deafness, ataxia, mental retardation, and electrolyte imbalance; Scholl et al., 2009) or EAST syndrome (Epilepsy, Ataxia, Sensorineural deafness, renal Tubulopathy; Bockenhauer et al., 2009). Interestingly, motor strength and nerve conduction velocity were also reduced in a patient in Scholl et al. (2009), suggesting the possibility that Kir4.1 expression in NMSC such as TPSC may affect neuromuscular function by regulating perisynaptic $[K^+]_o$ along nerves or at the NMJ. Consistent with this idea,.) exogenous K^+ depolarized TPSC in *ex vivo* neuromuscular preparations and b.) muscle fatigue was enhanced in mice in which this TPSC response to K^+ was reduced (Heredia et al., 2018). In order to address the physiological function of Kir4.1 in NMSC, future studies examining the effects of cell-specific deletion of the *KCNJ10* can be performed. These studies may shed light not only on the role of Kir4.1 in NMSC, but also in other populations of glia.

Acknowledgements

This work was supported with funds from the National Institutes of Health (NIH): 1 R21 NS 107922 (TWG) and GM103513 (Kent Sanders) as well as a faculty development award from the UNR Office of the Vice President of Research and Innovation (TWG). We thank Dave White for assistance with FACS, work which was performed in a Core laboratory supported by NIH grant GM103513. The authors have no conflict of interest. Data available on request from the authors.

References

Arthur-Farraj P, Moyon S. DNA methylation in Schwann cells and in oligodendrocytes. Glia. 2020 Aug;68(8):1568–1583. [PubMed: 31958184]

Barik A, Li L, Sathyamurthy A, Xiong WC, Mei L. Schwann Cells in Neuromuscular Junction Formation and Maintenance. J Neurosci. 2016 Sep 21;36(38):9770–81. [PubMed: 27656017]

Beckner ME. A roadmap for potassium buffering/dispersion via the glial network of the CNS. Neurochem Int. 2020 Jun;136:104727. [PubMed: 32194142]

Bin JM, Harris SN, Kennedy TE. The oligodendrocyte-specific antibody 'CC-1' binds Quaking 7. J Neurochem. 2016 Oct;139(2):181–186. [PubMed: 27454326]

Bindels RJ, Timmermans JA, Hartog A, Coers W, van Os CH. Calbindin-D9k and parvalbumin are exclusively located along basolateral membranes in rat distal nephron. J Am Soc Nephrol. 1991 Dec;2(6):1122–9. [PubMed: 1777592]

Bockenhauer D, Feather S, Stanescu HC, Bandulik S, Zdebik AA, Reichold M, Tobin J, Lieberer E, Sterner C, Landoure G, Arora R, Sirimanna T, Thompson D, Cross JH, van't Hoff W, Al Masri O, Tullus K, Yeung S, Anikster Y, Klootwijk E, Hubank M, Dillon MJ, Heitzmann D, Arcos-Burgos M, Knepper MA, Dobbie A, Gahl WA, Warth R, Sheridan E, Kleta R. Epilepsy, ataxia, sensorineural deafness, tubulopathy, and KCNJ10 mutations. N Engl J Med. 2009 May 7;360(19):1960–70. [PubMed: 19420365]

Brasko C, Hawkins V, De La Rocha IC, Butt AM. Expression of Kir4.1 and Kir5.1 inwardly rectifying potassium channels in oligodendrocytes, the myelinating cells of the CNS. Brain Struct Funct. 2017 Jan;222(1):41–59. [PubMed: 26879293]

Carroll SL, Ratner N. How does the Schwann cell lineage form tumors in NF1? Glia. 2008 Nov 1;56(14):1590–605. [PubMed: 18803326]

Castro R, Taetzsch T, Vaughan SK, Godbe K, Chappell J, Settlage RE, Valdez G. Specific labeling of synaptic schwann cells reveals unique cellular and molecular features. Elife. 2020 Jun 25;9:e56935. [PubMed: 32584256]

Darabid H, Perez-Gonzalez AP, Robitaille R. Neuromuscular synaptogenesis: coordinating partners with multiple functions. Nat Rev Neurosci. 2014 Nov;15(11):703–18. [PubMed: 25493308]

Djukic B, Casper KB, Philpot BD, Chin LS, McCarthy KD. Conditional knock-out of Kir4.1 leads to glial membrane depolarization, inhibition of potassium and glutamate uptake, and enhanced short-term synaptic potentiation. J Neurosci. 2007 Oct 17;27(42):11354–65. [PubMed: 17942730]

Espinosa-Medina I, Jevans B, Boismoreau F, Chettouh Z, Enomoto H, Müller T, Birchmeier C, Burns AJ, Brunet JF. Dual origin of enteric neurons in vagal Schwann cell precursors and the sympathetic neural crest. Proc Natl Acad Sci U S A. 2017 Nov 7;114(45):11980–11985. [PubMed: 29078343]

Faissner A, Kruse J, Nieke J, Schachner M. Expression of neural cell adhesion molecule L1 during development, in neurological mutants and in the peripheral nervous system. Brain Res. 1984 Jul;317(1):69–82. [PubMed: 6467033]

Feltri ML, D'Antonio M, Previtali S, Fasolini M, Messing A, Wrabetz L. P0-Cre transgenic mice for inactivation of adhesion molecules in Schwann cells. Ann N Y Acad Sci. 1999 Sep 14;883:116–23.

Feltri ML, Poitelon Y, Previtali SC. How Schwann Cells Sort Axons: New Concepts. Neuroscientist. 2016 Jun;22(3):252–65. [PubMed: 25686621]

Fricker FR, Zhu N, Tsantoulas C, Abrahamsen B, Nassar MA, Thakur M, Garratt AN, Birchmeier C, McMahon SB, Wood JN, Bennett DL. Sensory axon-derived neuregulin-1 is required for axoglial signaling and normal sensory function but not for long-term axon maintenance. J Neurosci. 2009 Jun 17;29(24):7667–78. [PubMed: 19535578]

George D, Ahrens P, Lambert S. Satellite glial cells represent a population of developmentally arrested Schwann cells. Glia. 2018 Jul;66(7):1496–1506. [PubMed: 29520852]

Gerber D, Pereira JA, Gerber J, Tan G, Dimitrieva S, Yángüez E, Suter U. Transcriptional profiling of mouse peripheral nerves to the single-cell level to build a sciatic nerve ATlas (SNAT). Elife. 2021 Apr 23;10:e58591. [PubMed: 33890853]

Gomez-Sanchez JA, Pilch KS, van der Lans M, Fazal SV, Benito C, Wagstaff LJ, Mirsky R, Jessen KR. After Nerve Injury, Lineage Tracing Shows That Myelin and Remak Schwann Cells Elongate Extensively and Branch to Form Repair Schwann Cells, Which Shorten Radically on Remyelination. J Neurosci. 2017 Sep 13;37(37):9086–9099. [PubMed: 28904214]

Griffin JW, Thompson WJ. Biology and pathology of nonmyelinating Schwann cells. Glia. 2008 Nov 1;56(14):1518–31. [PubMed: 18803315]

Hahn AF, Chang Y, Webster HD. Development of myelinated nerve fibers in the sixth cranial nerve of the rat: a quantitative electron microscope study. J Comp Neurol. 1987 Jun 22;260(4):491–500. [PubMed: 3611408]

Harty BL, Monk KR. Unwrapping the unappreciated: recent progress in Remak Schwann cell biology. Curr Opin Neurobiol. 2017;47:131–137. [PubMed: 29096241]

Hastings RL, Mikesh M, Lee YI, Thompson WJ. Morphological remodeling during recovery of the neuromuscular junction from terminal Schwann cell ablation in adult mice. Sci Rep. 2020 Jul 7;10(1):11132. [PubMed: 32636481]

Heredia DJ, Feng CY, Hennig GW, Renden RB, Gould TW. Activity-induced Ca^{2+} signaling in perisynaptic Schwann cells of the early postnatal mouse is mediated by $P2Y_1$ receptors and regulates muscle fatigue. Elife. 2018 Jan 31;7:e30839. [PubMed: 29384476]

Hibino H, Fujita A, Iwai K, Yamada M, Kurachi Y. Differential assembly of inwardly rectifying K+ channel subunits, Kir4.1 and Kir5.1, in brain astrocytes. J Biol Chem. 2004 Oct 15;279(42):44065–73. [PubMed: 15310750]

Higashi K, Fujita A, Inanobe A, Tanemoto M, Doi K, Kubo T, Kurachi Y. An inwardly rectifying K(+) channel, Kir4.1, expressed in astrocytes surrounds synapses and blood vessels in brain. Am J Physiol Cell Physiol. 2001 Sep;281(3):C922–31. [PubMed: 11502569]

Hornig J, Fröb F, Vogl MR, Hermans-Borgmeyer I, Tamm ER, Wegner M. The transcription factors Sox10 and Myrf define an essential regulatory network module in differentiating oligodendrocytes. PLoS Genet. 2013 Oct;9(10):e1003907. [PubMed: 24204311]

Jahromi BS, Robitaille R, Charlton MP. Transmitter release increases intracellular calcium in perisynaptic Schwann cells in situ. Neuron. 1992 Jun;8(6):1069–77. [PubMed: 1351731]

Jessen KR, Mirsky R. The origin and development of glial cells in peripheral nerves. Nat Rev Neurosci. 2005 Sep;6(9):671–82. [PubMed: 16136171]

Jessen KR, Mirsky R. Negative regulation of myelination: relevance for development, injury, and demyelinating disease. Glia. 2008 Nov 1;56(14):1552–65. [PubMed: 18803323]

Jessen KR, Mirsky R. Control of Schwann cell myelination. F1000 Biol Rep. 2010 Mar 15;2:19. [PubMed: 20948814]

Kalsi AS, Greenwood K, Wilkin G, Butt AM. Kir4.1 expression by astrocytes and oligodendrocytes in CNS white matter: a developmental study in rat optic nerve. J Anat. 2004 Jun;204(6):475–85. [PubMed: 15198689]

Kastriti ME, Kameneva P, Adameyko I. Stem cells, evolutionary aspects and pathology of the adrenal medulla: A new developmental paradigm. Mol Cell Endocrinol. 2020 Dec 1;518:110998. [PubMed: 32818585]

Kelley KW, Ben Haim L, Schirmer L, Tyzack GE, Tolman M, Miller JG, Tsai HH, Chang SM, Molofsky AV, Yang Y, Patani R, Lakatos A, Ullian EM, Rowitch DH. Kir4.1-Dependent Astrocyte-Fast Motor Neuron Interactions Are Required for Peak Strength. Neuron. 2018 Apr 18;98(2):306–319.e7. [PubMed: 29606582]

Kofuji P, Ceelen P, Zahs KR, Surbeck LW, Lester HA, Newman EA. Genetic inactivation of an inwardly rectifying potassium channel (Kir4.1 subunit) in mice: phenotypic impact in retina. J Neurosci. 2000 Aug 1;20(15):5733–40. [PubMed: 10908613]

Kucheryavykh YV, Kucheryavykh LY, Nichols CG, Maldonado HM, Baksi K, Reichenbach A, Skatchkov SN, Eaton MJ. Downregulation of Kir4.1 inward rectifying potassium channel subunits by RNAi impairs potassium transfer and glutamate uptake by cultured cortical astrocytes. Glia. 2007 Feb;55(3):274–81. [PubMed: 17091490]

Larsen BR, Assentoft M, Cotrina ML, Hua SZ, Nedergaard M, Kaila K, Voipio J, MacAulay N. Contributions of the Na^+/K^+-ATPase, NKCC1, and Kir4.1 to hippocampal K^+ clearance and volume responses. Glia. 2014 Apr;62(4):608–22. [PubMed: 24482245]

Larson VA, Mironova Y, Vanderpool KG, Waisman A, Rash JE, Agarwal A, Bergles DE. Oligodendrocytes control potassium accumulation in white matter and seizure susceptibility. Elife. 2018 Mar 29;7:e34829. [PubMed: 29596047]

Lau P, Verrier JD, Nielsen JA, Johnson KR, Notterpek L, Hudson LD. Identification of dynamically regulated microRNA and mRNA networks in developing oligodendrocytes. J Neurosci. 2008 Nov 5;28(45):11720–30. [PubMed: 18987208]

Leone DP, Genoud S, Atanasoski S, Grausenburger R, Berger P, Metzger D, Macklin WB, Chambon P, Suter U. Tamoxifen-inducible glia-specific Cre mice for somatic mutagenesis in oligodendrocytes and Schwann cells. Mol Cell Neurosci. 2003 Apr;22(4):430–40. [PubMed: 12727441]

Madadi A, Wolfart J, Lange F, Brehme H, Linnebacher M, Bräuer AU, Büttner A, Freiman T, Henker C, Einsle A, Rackow S, Köhling R, Kirschstein T, Müller S. Correlation between Kir4.1 expression and barium-sensitive currents in rat and human glioma cell lines. Neurosci Lett. 2021 Jan 10;741:135481. [PubMed: 33161102]

Maldonado PP, Vélez-Fort M, Levavasseur F, Angulo MC. Oligodendrocyte precursor cells are accurate sensors of local K+ in mature gray matter. J Neurosci. 2013 Feb 6;33(6):2432–42. [PubMed: 23392672]

Marcus DC, Wu T, Wangemann P, Kofuji P. KCNJ10 (Kir4.1) potassium channel knockout abolishes endocochlear potential. Am J Physiol Cell Physiol. 2002 Feb;282(2):C403–7. [PubMed: 11788352]

Nave KA, Werner HB. Myelination of the nervous system: mechanisms and functions. Annu Rev Cell Dev Biol. 2014;30:503–33. [PubMed: 25288117]

Neusch C, Rozengurt N, Jacobs RE, Lester HA, Kofuji P. Kir4.1 potassium channel subunit is crucial for oligodendrocyte development and in vivo myelination. J Neurosci. 2001 Aug 1;21(15):5429–38. [PubMed: 11466414]

Newman EA. Regional specialization of retinal glial cell membrane. Nature. 1984 May 10–16;309(5964):155–7. [PubMed: 6717594]

Nichols CG, Lopatin AN. Inward rectifier potassium channels. Ann Rev Physiol. 1997;59:171–91. [PubMed: 9074760]

Nishiyama A, Lin XH, Giese N, Heldin CH, Stallcup WB. Co-localization of NG2 proteoglycan and PDGF alpha-receptor on O2A progenitor cells in the developing rat brain. J Neurosci Res. 1996 Feb 1;43(3):299–314. [PubMed: 8714519]

Nwaobi SE, Lin E, Peramsetty SR, Olsen ML. DNA methylation functions as a critical regulator of Kir4.1 expression during CNS development. Glia. 2014 Mar;62(3):411–27. [PubMed: 24415225]

Nwaobi SE, Cuddapah VA, Patterson KC, Randolph AC, Olsen ML. The role of glial-specific Kir4.1 in normal and pathological states of the CNS. Acta Neuropathol. 2016 Jul;132(1):1–21. [PubMed: 26961251]

Olsen ML, Sontheimer H. Functional implications for Kir4.1 channels in glial biology: from K+ buffering to cell differentiation. J Neurochem. 2008;107(3):589–601. doi:10.1111/j.1471-4159.2008.05615. [PubMed: 18691387]

Orkand RK, Nicholls JG, Kuffler SW. Effect of nerve impulses on the membrane potential of glial cells in the central nervous system of amphibia. J Neurophysiol. 1966 Jul;29(4):788–806. [PubMed: 5966435]

Orkand RK. Extracellular potassium accumulation in the nervous system. Fed Proc. 1980 Apr;39(5):1515–8. [PubMed: 7364046]

Parmantier E, Lynn B, Lawson D, Turmaine M, Namini SS, Chakrabarti L, McMahon AP, Jessen KR, Mirsky R. Schwann cell-derived Desert hedgehog controls the development of peripheral nerve sheaths. Neuron. 1999 Aug;23(4):713–24. [PubMed: 10482238]

Poopalasundaram S, Knott C, Shamotienko OG, Foran PG, Dolly JO, Ghiani CA, Gallo V, Wilkin GP. Glial heterogeneity in expression of the inwardly rectifying K(+) channel, Kir4.1, in adult rat CNS. Glia. 2000 Jun;30(4):362–72. [PubMed: 10797616]

Procacci NM, Hastings RL, Aziz AA, Christensen NM, Zhao J, DeAngeli C, LeBlanc NM, Notterpek L, Valdez G, Gould TW. Data available upon request. 2020

Quintes S, Goebbels S, Saher G, Schwab MH, Nave KA. Neuron-glia signaling and the protection of axon function by Schwann cells. J Peripher Nerv Syst. 2010 Mar;15(1):10–6. [PubMed: 20433601]

Rangaraju S, Madorsky I, Pileggi JG, Kamal A, Notterpek L. Pharmacological induction of the heat shock response improves myelination in a neuropathic model. Neurobiol Dis 2008; 32(1):105–115. [PubMed: 18655835]

Rao M, Nelms BD, Dong L, Salinas-Rios V, Rutlin M, Gershon MD, Corfas G. Enteric glia express proteolipid protein 1 and are a transcriptionally unique population of glia in the mammalian nervous system. Glia. 2015 Nov;63(11):2040–2057. [PubMed: 26119414]

Reddy LV, Koirala S, Sugiura Y, Herrera AA, Ko CP. Glial cells maintain synaptic structure and function and promote development of the neuromuscular junction in vivo. Neuron. 2003 Oct 30;40(3):563–80. [PubMed: 14642280]

Reichenbach A, Derouiche A, Kirchhoff F. Morphology and dynamics of perisynaptic glia. Brain Res Rev. 2010 May;63(1–2):11–25. [PubMed: 20176054]

Rivera-Aponte DE, Melnik-Martínez KV, Malpica-Nieves CJ, Tejeda-Bayron F, Méndez-González MP, Skatchkov SN, Eaton MJ. Kir4.1 potassium channel regulation via microRNA-205 in astrocytes exposed to hyperglycemic conditions. Neuroreport. 2020 Apr 8;31(6):450–455. [PubMed: 32168096]

Robitaille R Modulation of synaptic efficacy and synaptic depression by glial cells at the frog neuromuscular junction. Neuron. 1998 Oct;21(4):847–55. [PubMed: 9808470]

Sapkota D, Dougherty JD. An inducible Cre mouse line to sparsely target nervous system cells, including Remak Schwann cells. Neural Dev. 2020 Feb 20;15(1):2. [PubMed: 32079539]

Scholl UI, Choi M, Liu T, Ramaekers VT, Häusler MG, Grimmer J, Tobe SW, Farhi A, Nelson-Williams C, Lifton RP. Seizures, sensorineural deafness, ataxia, mental retardation, and electrolyte imbalance (SeSAME syndrome) caused by mutations in KCNJ10. Proc Natl Acad Sci U S A. 2009 Apr 7;106(14):5842–7. [PubMed: 19289823]

Schirmer L, Möbius W, Zhao C, Cruz-Herranz A, Ben Haim L, Cordano C, Shiow LR, Kelley KW, Sadowski B, Timmons G, Pröbstel AK, Wright JN, Sin JH, Devereux M, Morrison DE, Chang SM, Sabeur K, Green AJ, Nave KA, Franklin RJ, Rowitch DH. Oligodendrocyte-encoded Kir4.1 function is required for axonal integrity. Elife. 2018 Sep 11;7:e36428. [PubMed: 30204081]

Schram G, Pourrier M, Wang Z, White M, Nattel S. Barium block of Kir2 and human cardiac inward rectifier currents: evidence for subunit-heteromeric contribution to native currents. Cardiovasc Res. 2003 Aug 1;59(2):328–38. [PubMed: 12909316]

Smith SE, Chen X, Brier LM, Bumstead JR, Rensing NR, Ringel AE, Shin H, Oldenborg A, Crowley JR, Bice AR, Dikranian K, Ippolito JE, Haigis MC, Papouin T, Zhao G, Wong M, Culver JP, Bonni A. Astrocyte deletion of α2-Na/K ATPase triggers episodic motor paralysis in mice via a metabolic pathway. Nat Commun. 2020 Dec 2;11(1):6164. [PubMed: 33268780]

Son YJ, Thompson WJ. Schwann cell processes guide regeneration of peripheral axons. Neuron. 1995 Jan;14(1):125–32. [PubMed: 7826630]

Song P, Groos S, Riederer B, Feng Z, Krabbenhöft A, Manns MP, Smolka A, Hagen SJ, Neusch C, Seidler U. Kir4.1 channel expression is essential for parietal cell control of acid secretion. J Biol Chem. 2011 Apr 22;286(16):14120–8. [PubMed: 21367857]

Song F, Hong X, Cao J, Ma G, Han Y, Cepeda C, Kang Z, Xu T, Duan S, Wan J, Tong X. Kir4.1 channels in NG2-glia play a role in development, potassium signaling, and ischemia-related myelin loss. Commun Biol. 2018 Jun 28;1:80. [PubMed: 30271961]

Su G, Kintner DB, Flagella M, Shull GE, Sun D. Astrocytes from Na(+)-K(+)-Cl(−) cotransporter-null mice exhibit absence of swelling and decrease in EAA release. Am J Physiol Cell Physiol. 2002 May;282(5):C1147–60. [PubMed: 11940530]

Su XT, Wang WH. The expression, regulation, and function of Kir4.1 (Kcnj10) in the mammalian kidney. Am J Physiol Renal Physiol. 2016 Jul 1;311(1):F12–5. [PubMed: 27122539]

Sun W, Cornwell A, Li J, Peng S, Osorio MJ, Aalling N, Wang S, Benraiss A, Lou N, Goldman SA, Nedergaard M. SOX9 Is an Astrocyte-Specific Nuclear Marker in the Adult Brain Outside the Neurogenic Regions. J Neurosci. 2017 Apr 26;37(17):4493–4507. [PubMed: 28336567]

Takumi T, Ishii T, Horio Y, Morishige K, Takahashi N, Yamada M, Yamashita T, Kiyama H, Sohmiya K, Nakanishi S, et al. A novel ATP-dependent inward rectifier potassium channel expressed predominantly in glial cells. J Biol Chem. 1995 Jul 7;270(27):16339–46. [PubMed: 7608203]

Tang X, Taniguchi K, Kofuji P. Heterogeneity of Kir4.1 channel expression in glia revealed by mouse transgenesis. Glia. 2009 Dec;57(16):1706–15. [PubMed: 19382212]

Thuringer D, Chanteloup G, Boucher J, Pernet N, Boudesco C, Jego G, Chatelier A, Bois P, Gobbo J, Cronier L, Solary E, Garrido C. Modulation of the inwardly rectifying potassium channel Kir4.1 by the pro-invasive miR-5096 in glioblastoma cells. Oncotarget. 2017 Jun 6;8(23):37681–37693. [PubMed: 28445150]

Uesaka T, Nagashimada M, Enomoto H. Neuronal Differentiation in Schwann Cell Lineage Underlies Postnatal Neurogenesis in the Enteric Nervous System. J Neurosci. 2015 Jul 8;35(27):9879–88. [PubMed: 26156989]

Weaver CD, Denton JS. Next-generation inward rectifier potassium channel modulators: discovery and molecular pharmacology. Am J Physiol Cell Physiol. 2021 Jun 1;320(6):C1125–C1140. [PubMed: 33826405]

Main Points

Kir4.1-CreER^{T2} mice were developed to track Kir4.1 expression.

Using this genetic tool, we observed that Kir4.1 is initially expressed in immature Schwann cells, downregulated in myelinating Schwann cells and maintained in non-myelinating Schwann cells of peripheral nerves and at the NMJ.

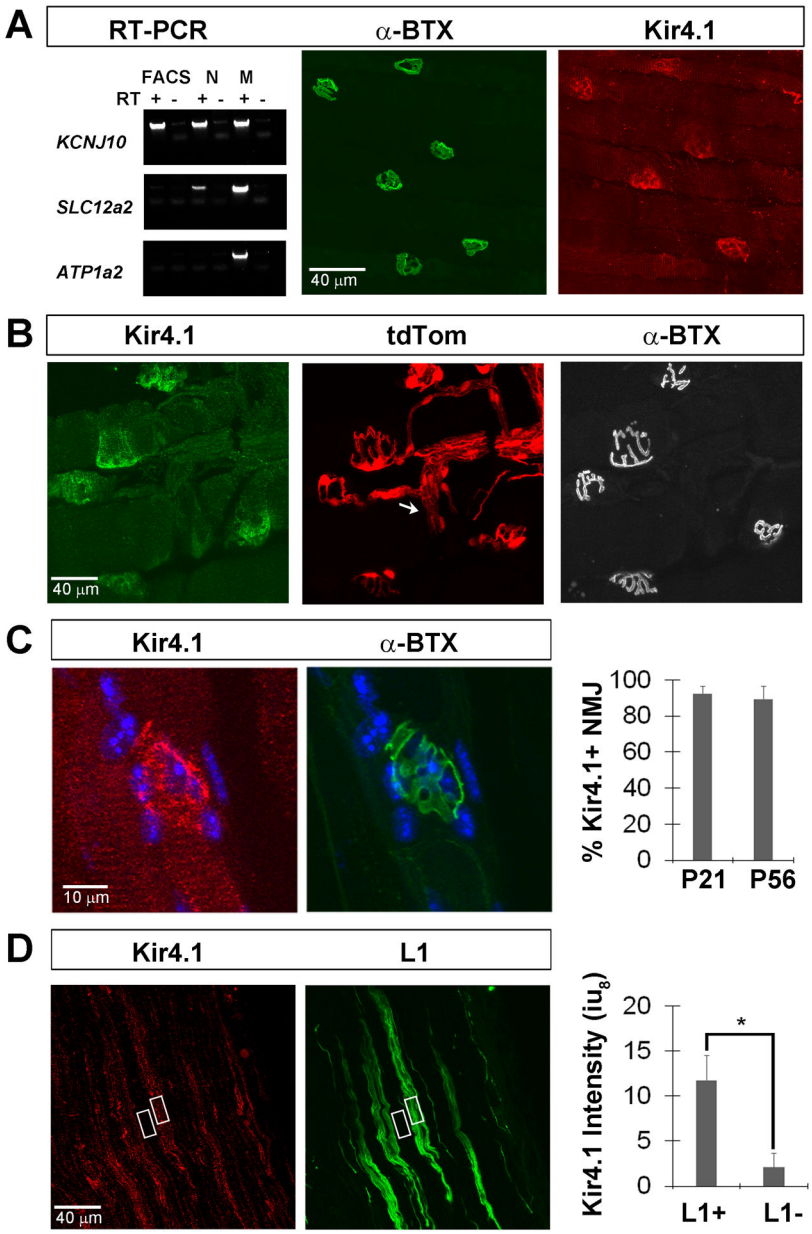

Figure 1. The inwardly-rectifying potassium channel Kir4.1 is expressed in non-myelinating Schwann cells, including terminal/perisynaptic Schwann cells (TPSC) at the neuromuscular junction (NMJ).

A, Expression of *KCNJ10* (encoding Kir4.1), *SLC12a2* (encoding NKCC1 or $Na^+/K^+/Cl^-$ cotransporter) and *ATP1a2* (encoding Na^+/K^+ ATPase α2), in P7 Schwann cells sorted by FACS from the diaphragm muscle of *Sox10-tdTomato* mice (FACS), P7 phrenic nerve (N) and P7 diaphragm muscle (M). *KCNJ10* is expressed by all three samples, *SLC12a2* by nerve and muscle samples, and *APA1a2* by the muscle sample (left panel). Immunohistochemical staining of Kir4.1 (red) at AlexaFluor 488-conjugated α-BTX-labeled AChR clusters (green) in adult (P56) diaphragm muscle of wild-type mice (middle and right panels). ***B***, Immunohistochemical staining of Kir4.1 (green) at AlexaFluor 633-conjugated α-BTX-labeled AChR clusters (white) in adult (P56) diaphragm muscle of *Sox10-tdTomato*

mice in which SC are labeled with the fluorescent protein tdTomato (red). Kir4.1 is found in tdTomato-positive (tdTom+) TPSC at α-BTX-labeled NMJ, but not in tdTomato-positive SC along distal nerve branches innervating the NMJ (arrow). ***C***, Higher magnification image of Kir4.1 (red), α-BTX (green) and Hoechst (blue) staining of NMJ in the diaphragm (left and middle panel). Percentage of α-BTX-labeled NMJ exhibiting Kir4.1 immunoreactivity in the diaphragm of P21 and adult (P56) wild-type mice (right panel; P21: n=3; 2M,1F; c=35/n; P56: n=4; 2M,2F; c=40/n). ***D***, Immunohistochemical staining of Kir4.1 (red) and L1-labeled RSC (green) in longitudinal sections of adult sciatic nerve of wild-type mice (left and middle panel). Kir4.1 immunofluorescence intensity (8-bit intensity units; iu_8) per 200-μm^2 rectangles in L1+ (right rectangle) and L1− (left rectangle) regions (right panel; n=4; 2M,2F; rectangles=6/n; *P=0.0000189, 2-tailed, unpaired Student's t).

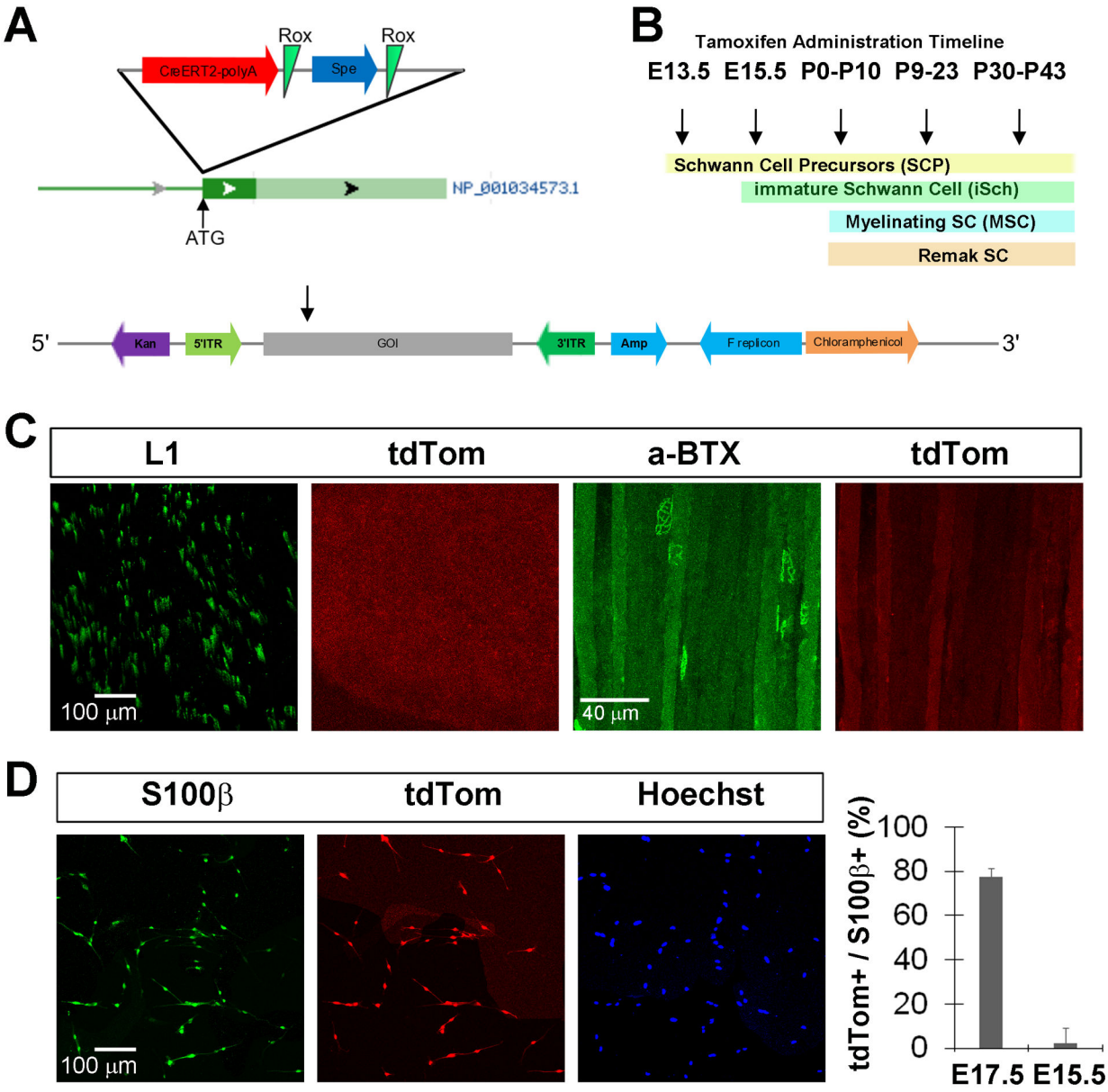

Figure 2. BAC transgenic *Kir4.1-CreER^{T2}* mice do not exhibit tamoxifen-independent expression.

A, A CreER^{T2}-polyA construct, together with a Rox-flanked spectinomycin selection cassette, was cloned upstream of the ATG of the Kir4.1-encoding gene *KCNJ10* (NCBI reference sequence NP_001034573.1) in the RP24–295K5 BAC by homologous recombination (HR). PiggyBAC inverted terminal repeats (ITRs) were inserted by HR into the BAC backbone flanking the genomic insert of CreER^{T2} (gene of interest or GOI) in order to facilitate the transposase-mediated integration of the targeted BAC into the host genome. ***B***, Timeline of tamoxifen (TMX) administration schemes utilized in this study and the correlated stages of Schwann cell development. ***C***, tdTom expression was not observed in L1-labeled sciatic nerve sections (left two panels) or AlexaFluor 488-conjugated α-BTX-labeled diaphragm whole mounts (right tow panels) of adult Kir4.1-CreER^{T2}, conditional tdTomato mice (*Kir4.1-tdTomato*) in the absence of TMX treatment. ***D***, Most S100β-labeled

SC isolated from the sciatic nerves of P0 *Kir4.1-tdTomato* mice whose mothers were injected with TMX at E17.5 and E18.5 exhibit tdTom expression (left three panels). Percentage of S100β-labeled SC expressing tdTom after embryonic TMX administration at E17.5 and E18.5 (E17.5) or at E15.5 (right panel); data in text.

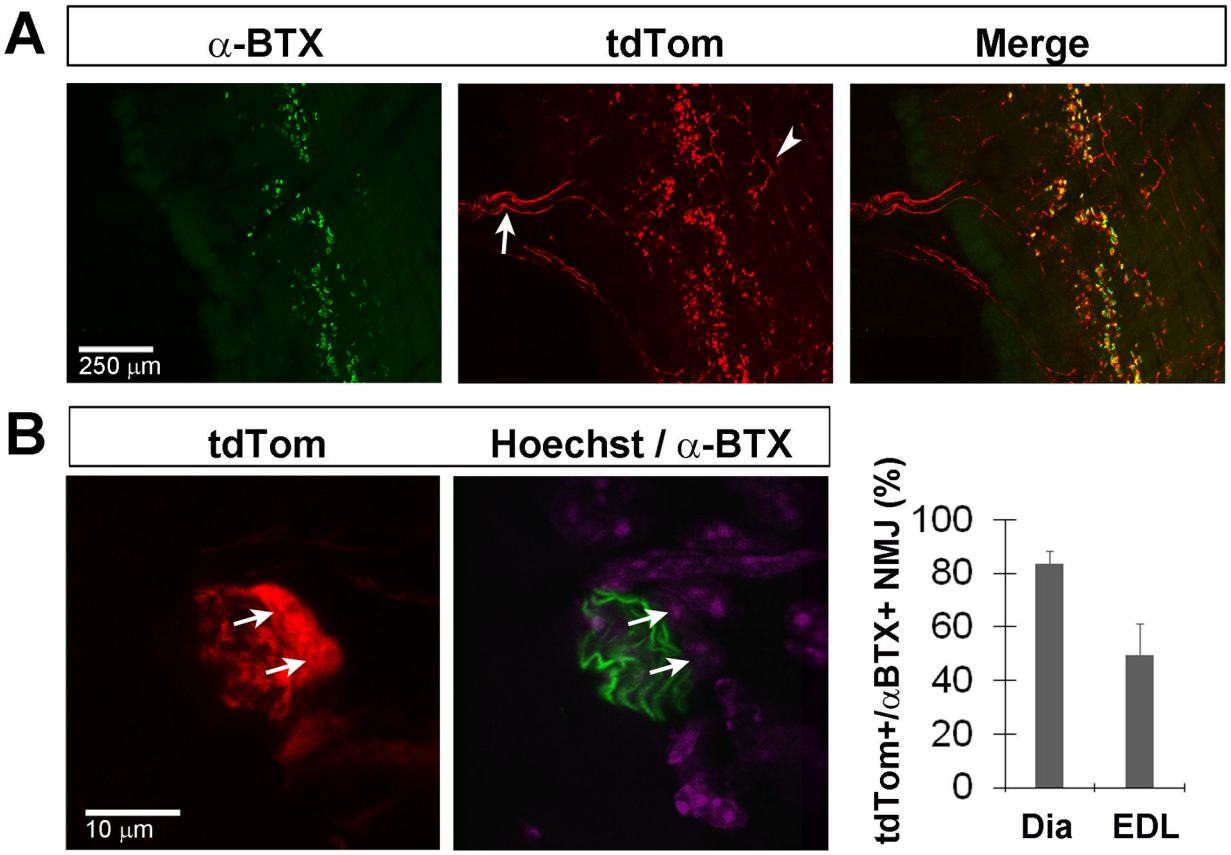

Figure 3. ***Kir4.1-tdTomato*** **mice given TMX at post-weaning stages exhibit tdTom expression in TPSC of the diaphragm as well as in some cells of the phrenic nerve.**

A, Low-magnification images of the diaphragm muscle from P50 *Kir4.1-tdTomato* mice given TMX from P30-P43 show tdTom+ TPSC at AlexaFluor 488-conjugated α-BTX-labeled AChR clusters (arrowhead), but also in cells associated with phrenic nerve (arrow). ***B***, Diaphragm muscle from P25 *Kir4.1-tdTomato* mice given TMX from P9-P22 shows tdTomato expression (red) by two Hoechst-labeled nuclei (arrows, purple) near AlexaFluor 488-conjugated α-BTX-labeled AChR clusters (green) in the left and middle panel. Percentage of TPSC at α-BTX-labeled NMJ expressing tdTom in the diaphragm and EDL muscles after TMX from P30-P43 (right panel); data in text.

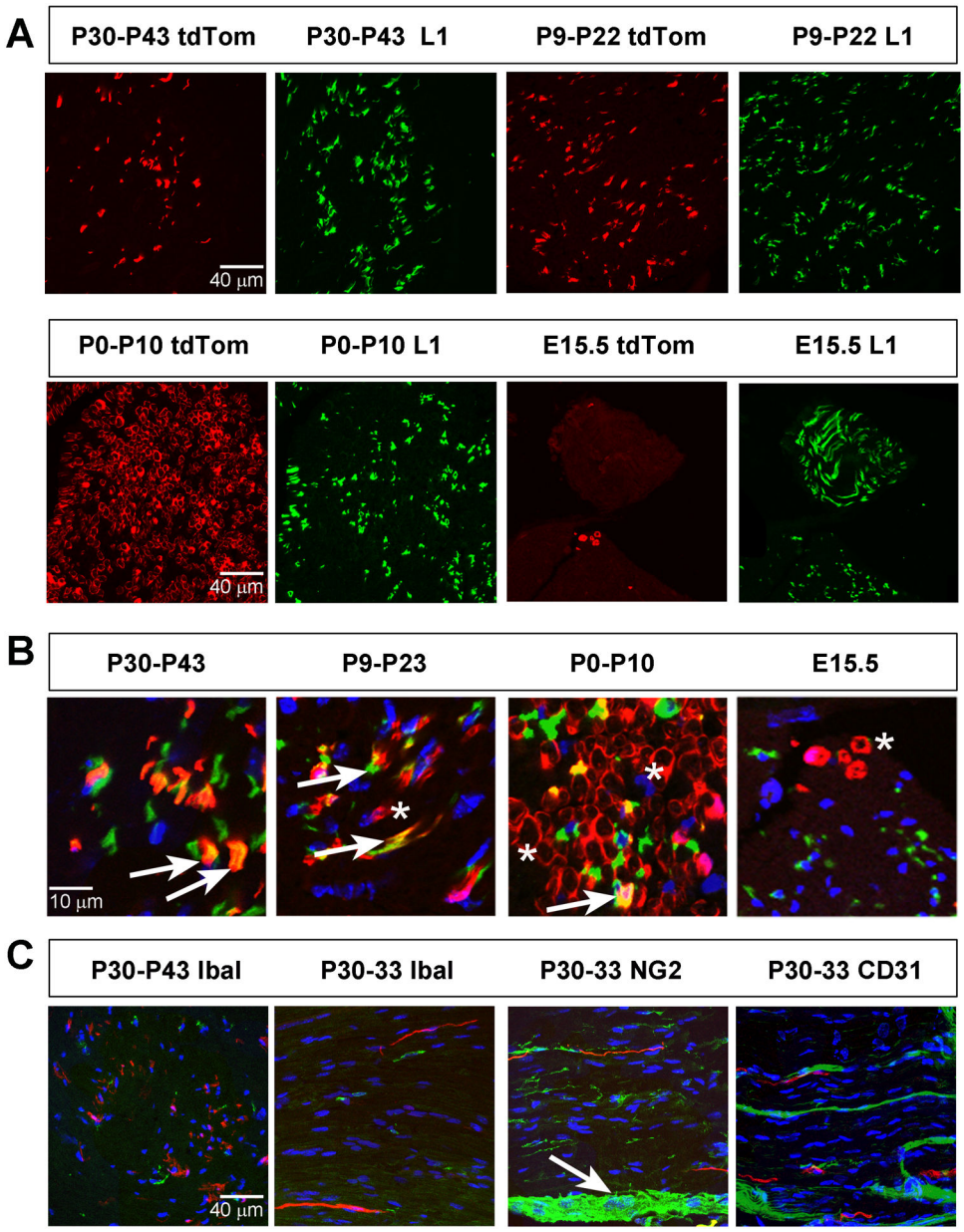

Figure 4. ***Kir4.1-tdTomato*** **mice given TMX at stages after the end of myelination onset exhibit tdTom+ cells in L1+ Remak Schwann cells (RSC) of sciatic nerve.**

A, Images of sciatic nerve cross sections from P50 *Kir4.1-tdTomato* mice given TMX from P30-P43 (left two panels, top row) or from P9-P22 (right two panels, top row) show tdTom+ cells (red) that co-localize with L1+ RSC (green). In contrast, most tdTom+ cells fail to co-localize with L1 when TMX is given from P0-P10 or from E14-E15 (bottom row). ***B***, High-magnification merged images of tdTom+ cells and L1+ RSC after each of the four TMX treatment regimes. Arrows show double-positive cells and asterisks show tdTom+, L1− cells. ***C***, Cross section (left panel) and longitudinal sections (next three panels) of sciatic nerve from P50 *Kir4.1-tdTomato* mice given TMX from P30-P43 (left panel) or P30-P33 (next three panels), stained with Iba1 to label macrophage (left two panels), NG2 to

stain endoneurial, perineurial and epineurial fibroblasts, and CD31 to stain endothelial cells. Arrow indicates epineurium.

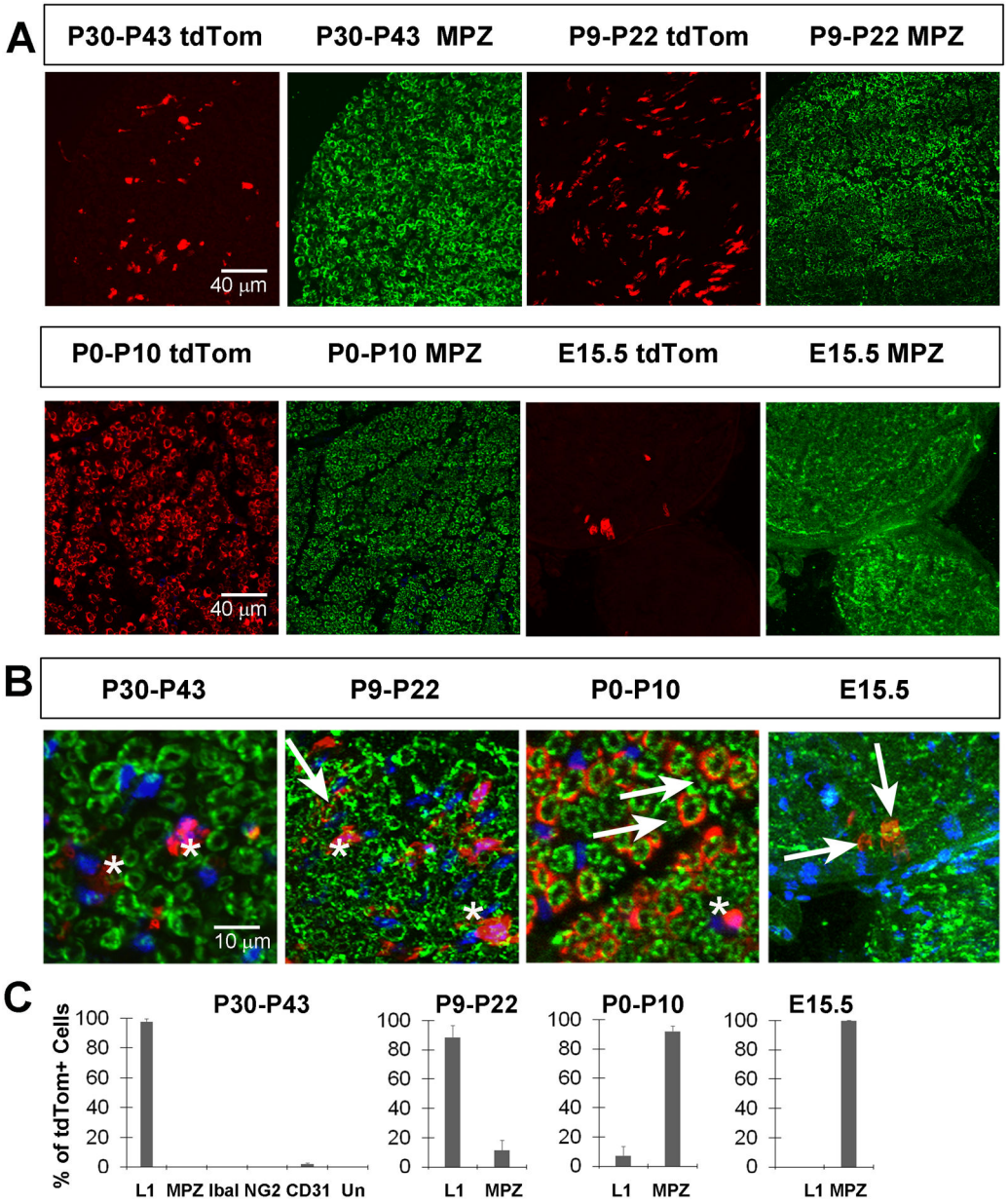

Figure 5. *Kir4.1-tdTomato* mice given TMX around the onset of myelination or before the end of myelination onset exhibit tdTom+ cells in MPZ+ myelinating Schwann cells (MSC).

A, Images of sciatic nerve cross sections from P50 *Kir4.1-tdTomato* mice given TMX from P30-P43 (left two panels, top row) or from P9-P22 (right two panels, top row) show tdTom+ cells (red) that fail to co-localize with MPZ+ MSC (green). In contrast, most tdTom+ cells co-localize with MPZ when TMX is given from P0-P10 or from E14-E15. ***B***, High-magnification merged images of tdTomato+ cells and MPZ+ myelinating SC after each of the four TMX treatment regimes. Arrows show double-positive cells and asterisks show tdTom+, MPZ− cells. ***C***, Percentage of tdTom+ cells in sciatic nerve at P50 that express L1, MPZ, Iba1, NG2 or CD31 in mice given TMX from P30-P43 or that express L1 or MPZ in mice given TMX from P9–22, P0-P10 or at E15.5; data in text.

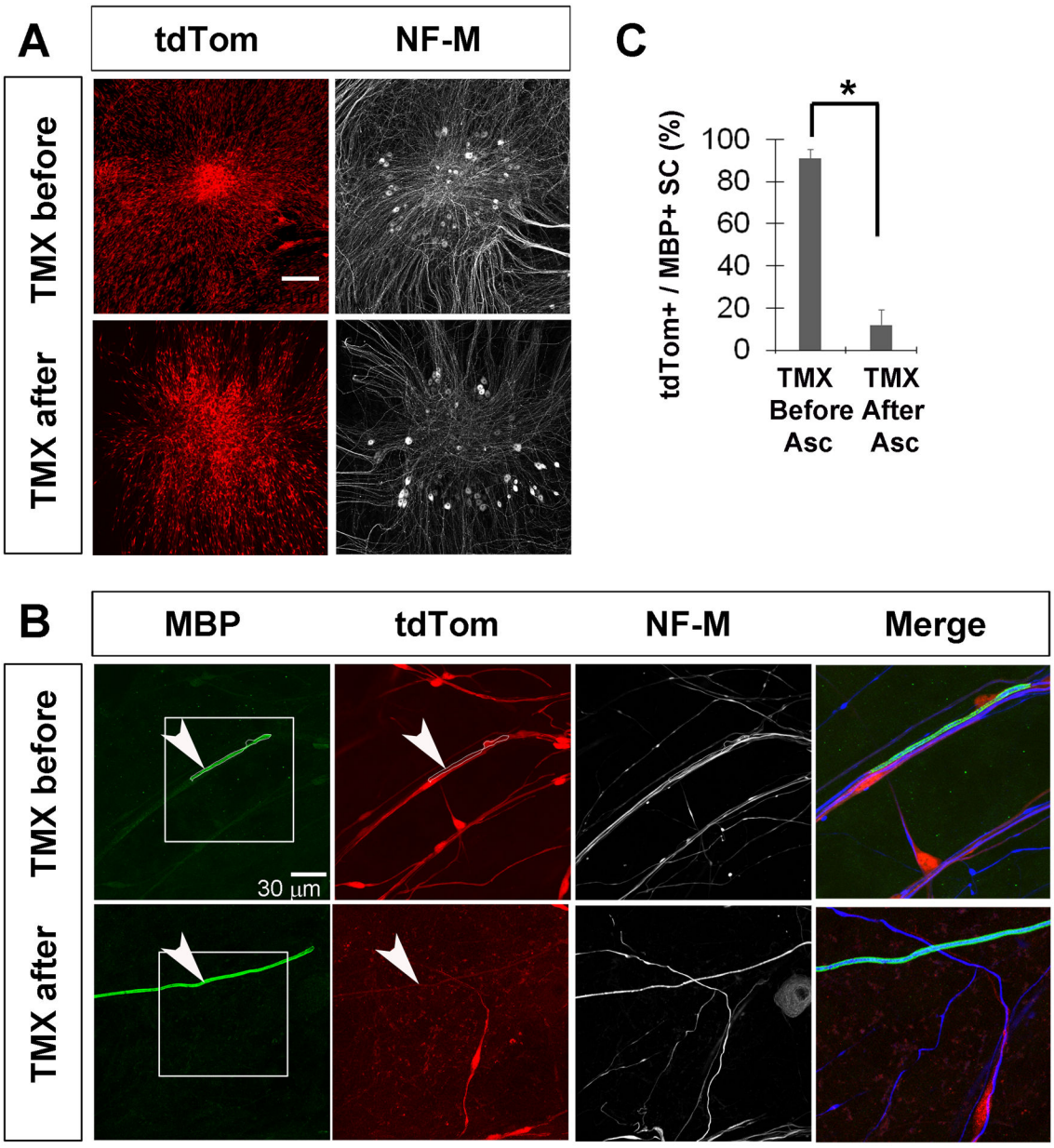

Figure 6. tdTomato is not expressed by Schwann cells derived from Kir4.1-CreER^{T2} mice that have been induced to myelinate *in vitro*.

A, Low-magnification images of DRG explant cultures show extensive tdTom+ SC associated with DRG after addition of TMX either before or after the induction of myelination by ascorbate. ***B***, An MBP-positive MSC (outlined in white) associated with a neurofilament-M (NF-M)-reactive neurite expresses tdTom when TMX was added before ascorbate (top row), showing that Kir4.1 was robustly expressed in this cell before myelination was induced. In contrast, neurite-associated SC failed to express tdTom when TMX was added after ascorbate, demonstrating that Cre activity in Kir4.1-CreER^{T2} mice was downregulated in response to myelination. *C*, Percentage of MBP+ Schwann cells expressing tdTom when tamoxifen was given before or after ascorbate; data in text. Expressing and non-expressing SC were defined as ones in which the tdTom fluorescence

intensity within a 4 μm^2 square overlapping an MBP+ region was greater than 30 or less than 20 iu_8.

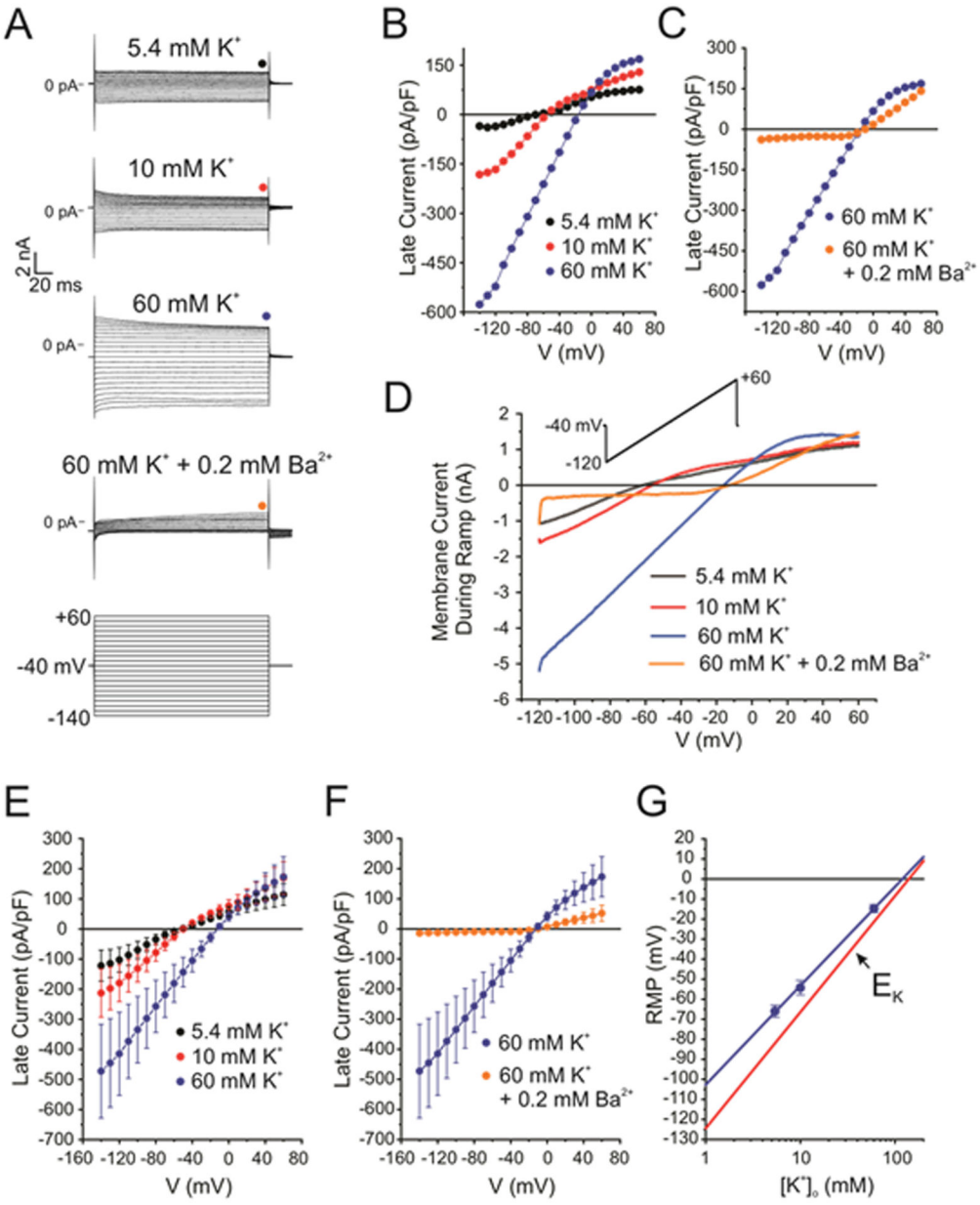

Figure 7. Acutely dissociated NMSC of the sciatic nerve exhibit a large barium-sensitive inwardly rectifying conductance that is consistent with the expression of Kir4.1 channels.

A, Typical whole-cell patch clamp experiment demonstrating the existence of inwardly rectifying K^+ channels in mouse NMSC. The four top families of macroscopic currents were recorded in the same cell under the conditions indicated above each set of traces. These were elicited in response to the voltage clamp protocol shown at the bottom. The colored circles above each set of traces indicate at which time point the current was measured to construct the I-V relationships shown in panels ***B*** and ***C***. ***B***, Notice the large increase of the inward current as external K^+ concentration ($[K^+]_o$) was progressively raised from 5.4 (Control; black circles) to 10 (red circles) and then 60 (blue circles) mM. ***C***, The large inward current recorded in 60 mM $[K^+]_o$ was potently inhibited by cell exposure to 0.2 mM Ba^{2+} (orange circles). ***D***, I-V relationships generated in the same cell as that in panel ***A*** in the presence

of 5.4 (black line), 10 (red line) or 60 (blue line) mM $[K^+]_o$, or 60 mM $[K^+]_o$ + 0.2 mM Ba^{2+} (orange line) in response to the voltage ramp protocol shown above as an inset. ***E***, Mean I-V relationships recorded in the presence of 5.4 (black circles; *n*=6), 10 (red circles; *n*=4; c=4) or 60 mM (blue circles; *n*=3; *c*=3) $[K^+]_o$. Each data point is a mean ± s.e. ***F***, Mean I-V relationships generated in the presence of 60 mM $[K^+]_o$ (blue circles; n=3), or 60 mM $[K^+]_o$ + 0.2 mM Ba^{2+} (orange circles; *n*=4; *c*=5). Each data point is a mean ± s.e. ***G***, Near Nernstian behavior of the resting membrane potential (RMP) in mouse NMSC. Each blue data point is the mean ± SEM RMP recorded in the presence of 5.4 (*n*=5; *c*=6), 10 (*n*=4; *c*=4) or 60 (*n*=4; *c*=4) mM $[K^+]_o$. The solid blue line is a least-square linear fit to the data points that included the error bars as weights. The slope of this line was 49.4 ± 1.0 mV/decade (r^2 = 0.9996). The solid red line is the estimated equilibrium potential for K^+ (E_K) in our conditions, which was calculated using the Nernst equation (RT/zF = 58 mV/decade) with an internal K^+ concentration = 140 mM.

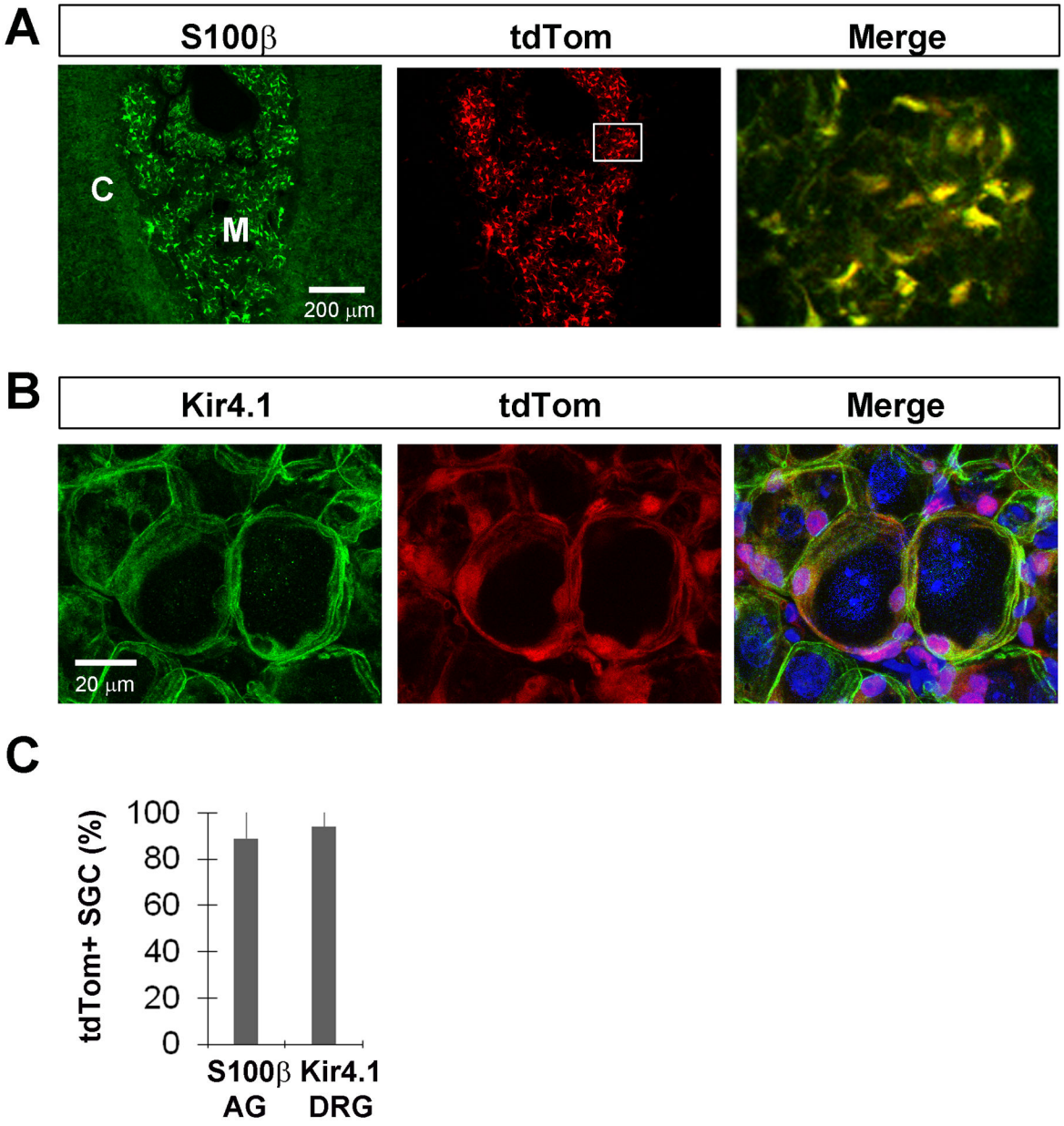

Figure 8. ***Kir4.1-tdTomato*** **mice given TMX at post-weaning stages exhibit tdTom expression in non-myelinating satellite glial cells (SGC) of the adrenal medulla and dorsal root ganglia.**

A, S100β-positive SGC of the adrenal medulla express tdTom when TMX was given at P30-P43. Merge represents the inset box. ***B***, Kir4.1-immunoreactive SGC of the lumbar 4 (L4) dorsal root ganglia (DRG) also express tdTom when TMX was given at P30-P43. ***C***, Percentage of S100β+ SGC in medulla of adrenal gland (AG; 89 ± 13.1%; *n*=4; 2M,2F; *c*=63/*n*) or Kir4.1+ SGC of L4 DRG (94.2 ± 8.3%; *n*=4; 2M,2F; *c*=42/*n*) that express tdTom after TMX from P30-P43.

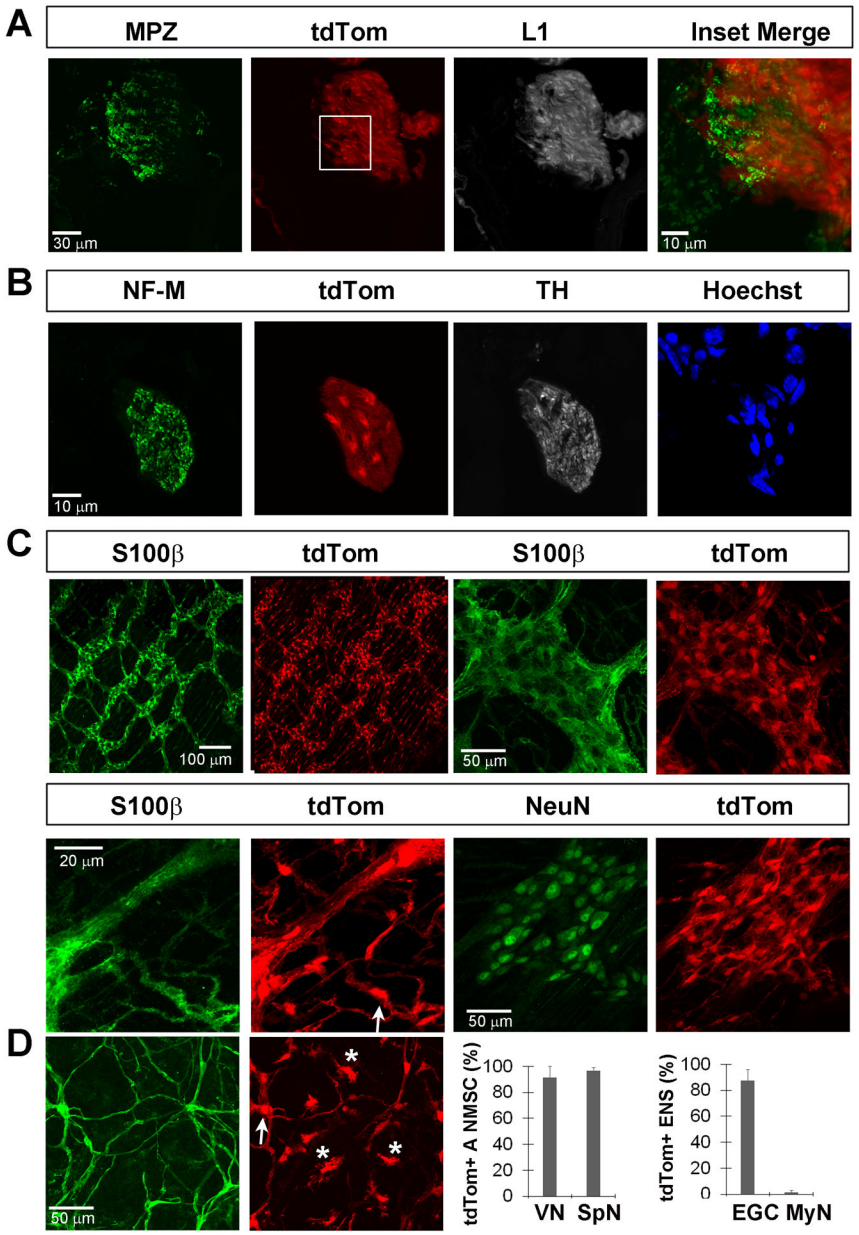

Figure 9. ***Kir4.1-tdTomato*** **mice given TMX at post-weaning stages exhibit tdTom expression in non-myelinating Schwann cells (NMSC) of autonomic nerves and enteric glial cells (EGC) of myenteric ganglia.**

A, L1+ NMSC, but not MPZ+ MSC, of the parasympathetic cervical vagus nerve trunk express tdTomato when TMX was given at P30-P43. ***B***, Cells of the non-myelinating sympathetic splenic nerve, identified just outside the spleen in sections by its association with tyrosine hydroxylase (TH), NF-M double-positive axons, express tdTom when TMX was given at P30-P43. ***C***, S100β-positive EGC within the myenteric ganglia of the colon express tdTom when TMX was given at P30-P43, as shown in low- and high-magnification images (top row, left and right two panels, respectively). tdTom was also expressed by S100β-positive EGC associated with the axons of these myenteric neurons as they course through the colonic smooth muscle (bottom row, left two panels). tdTom was not expressed

by NeuN+ myenteric neurons (bottom row, right two panels). ***D***, tdTom was expressed by S100β-positive EGC of the mucosa (arrows) but also expressed by a population of S100β-negative cells (asterisks; left two panels). Percentage of L1+ autonomic non-myelinating Schwann cells (A NMSC) of the vagus nerve (VN; 92.3 ± 7%; *n*=4; 2M,2F; *c*=12/*n*) or the splenic nerve (SpN; 96.8 ± 2.7%; *n*=4; 2M,2F; *c*=7/*n*) that express tdTom after TMX from P30-P43 (middle right panel). Percentage of S100β+ myenteric EGC of the enteric nervous system / ENS (EGC; 87.5 ± 8.7%; *n*=4; 2M,2F; *c*=54/*n*) or NeuN+ myenteric neurons (MyN: 1.25 ± 1.5%; *n*=4; 2M,2F; *c*=48/*n*) that express tdTom after TMX from P30-P43 (far right panel).

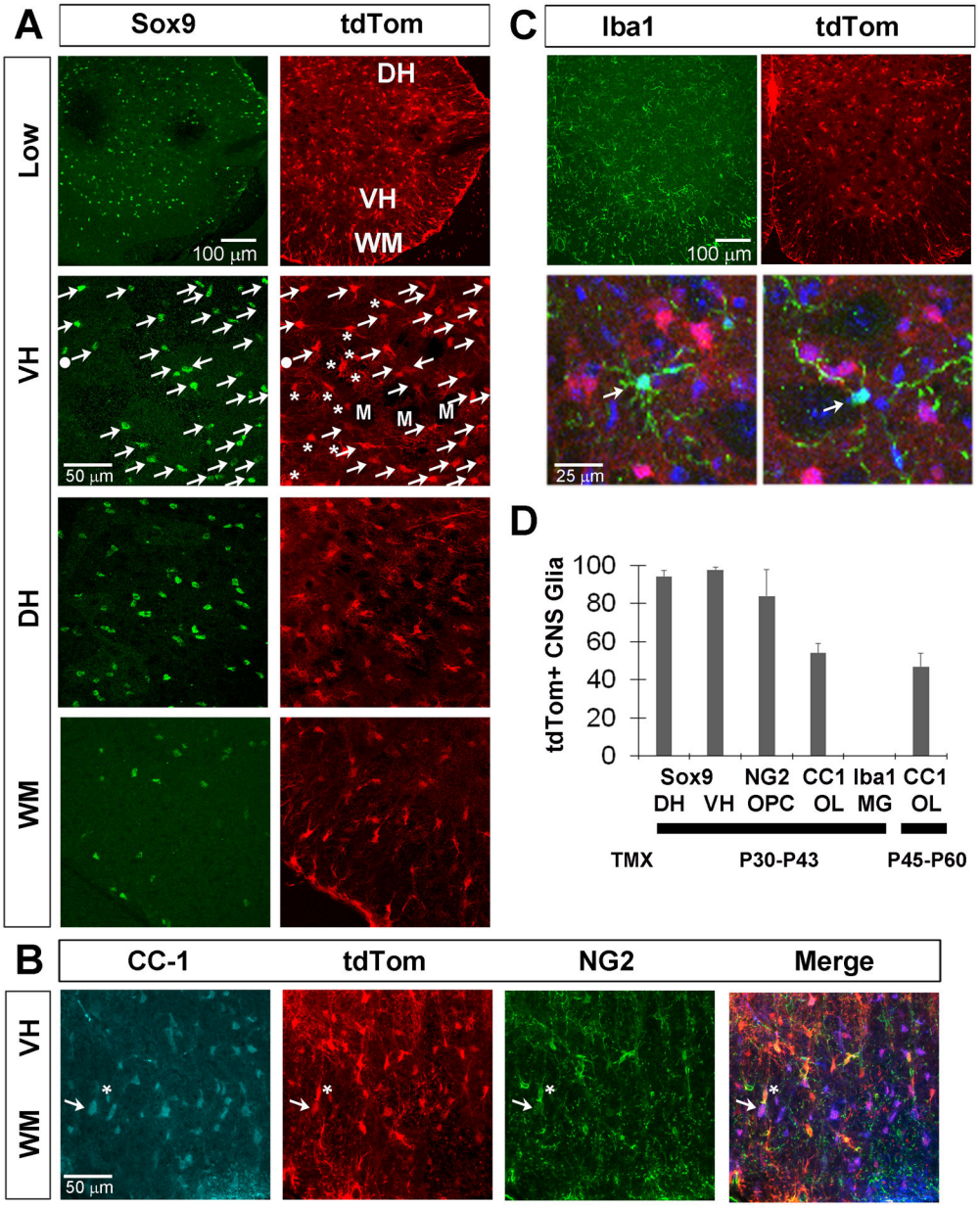

Figure 10. ***Kir4.1-tdTomato*** **mice given TMX at post-weaning stages exhibit tdTom expression in non-myelinating astrocytes and oligodendrocyte precursor cells (OPC) as well as myelinating oligodendrocytes (OL) in the spinal cord.**

A, Sox9+ astrocytes express tdTom in a low-magnification image of the spinal cord (top row) as well as in high-magnification images of the ventral horn (VH), dorsal horn (DH) and ventral white matter (WM; bottom three rows). In the VH, Sox9, tdTom double-labeled cells are indicated by arrows, tdTomato+, Sox9-negative cells by asterisks, and one tdTom-negative, Sox9+ cell by filled circle. Dark spaces indicate motor neuron nuclei (M). ***B***, tdTom+ cells also co-localize with NG2+ OPC (asterisk) and CC-1+ OLs (arrow). ***C***, Low-magnification separated and high-magnification merged images (top and bottom row) show that tdTom+ cells (red) do not express the microglial (MG) marker Iba1 (green); blue in bottom row = Hoechst-stained nuclei. ***D***, Percentage of Sox9+ astrocytes, NG2+ OPC,

CC-1+ OL or Iba1+ MG that express tdTom in spinal cord at P50 in mice given TMX from P30-P43 or of CC-1+ OL that express tdTom in spinal cord at P70 in mice given TMX from P45-P60; data in text. Sox9 numbers were separately calculated for dorsal and ventral horns (DH, VH).

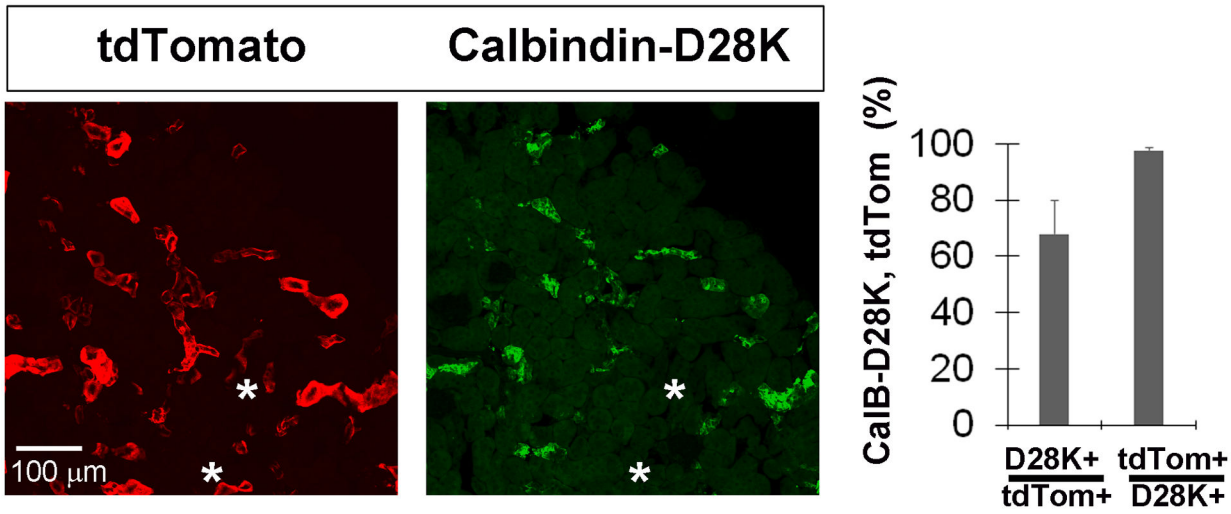

Figure 11. ***Kir4.1-tdTomato*** **mice given TMX at post-weaning stages exhibit tdTom expression in Calbindin-D28K+ renal epithelial cells of the distal convoluted tubule.**

A, Images of cross sections of the kidney from *Kir4.1-tdTomato* mice given TMX from P30-P43 co-stained with antibodies against calbindin-D28K (CalB-D28K), a marker for renal epithelial cells of the distal convoluted tubule (left and middle panel). Note the presence of tdTom+ cells that do not co-label with D28K (asterisks). Percentage of tdTom+ cells that express CalB-D28K, and percentage of CalB-D28K+ cells that express tdTom, in kidney at P50 in *Kir4.1-tdTomato* mice given TMX from P30-P43; data in text.